A Distributed Power-Allocation and Signal-Shaping Game for the Competitively Optimal Throughput-Maximization of Multiple-Antenna "*ad hoc*" Networks

Enzo Baccarelli, Mauro Biagi, *Member, IEEE*, and Cristian Pelizzoni

***Abstract*—This paper focuses on the competitively optimal power control and signal shaping for "*ad hoc*" networks composed by multiple-antenna noncooperative transmit/receive terminals affected by spatially colored multiple-access interference (MAI). The target is the competitive maximization of the information throughput sustained by each link that is active over the network. For this purpose, the MAI-impaired network is modeled as a noncooperative strategic game, and sufficient conditions for the existence and uniqueness of the Nash equilibrium (NE) are provided. Furthermore, iterative power-control and signal-shaping algorithms are presented to efficiently achieve the NE under both best-effort and "contracted QoS" policies. The presented algorithms also account for the effect of (possibly) imperfect channel estimates available at the transmit/receive units active over the network, they are fully scalable, and they may be implemented in a fully distributed and asynchronous way. The presented numerical results support the conclusion that the proposed distributed algorithms may be able to outperform the conventional centralized orthogonal MAC strategies (as time division multiple access, frequency division multiple access, and code division multiple access) in terms of a sustained network throughput, especially in operating scenarios affected by a strong MAI.**

***Index Terms*—Competitive optimality, game theory, multiple-access interference (MAI), multiple antennas, power allocation, spatial signal shaping.**

I. State of Art and Goals of the Work

DUE TO THE increasing demand for pervasive high-throughput personal communication services (PCSs), the requirement for "always-on" mobile access based on uncoordinated "*ad hoc*"-type networking architectures is expected to dramatically increase within the next few years [9]. To satisfy the resulting demand for a large network throughput, the spatial dimension provided by wireless multiantenna terminals may be exploited [10]. As a consequence, an increasing attention has been paid to the development of next-generation array-equipped transceivers for wireless PCSs [10].

Manuscript received September 15, 2004; revised July 23, 2005 and December 31, 2005. This work was supported in part by the National project Wireless 8O2.16 Multi-antenna mEsh Networks (WOMEN) under Grant 2005093248. The review of this paper was coordinated by Prof. Z. Wang.

The authors are with the INFO-COM Department, University of Rome "La Sapienza," 00184 Rome, Italy (e-mail: enzobac@infocom.uniroma1.it; biagi@infocom.uniroma1.it; pelcris@infocom.uniroma1.it).

Color versions of Figs. 1 and 3–7 are available at http://ieeexplore.ieee.org.
Digital Object Identifier 10.1109/TVT.2006.878565

A. Related Works and Proposed Contributions

Power control and spatial signal shaping are central issues for the optimized design of multiple-access interference (MAI)-limited "*ad hoc*" networks. In fact, in these networks, the information throughput (measured in bits/slot), which is conveyed by each link, depends on the power allocation and signal shaping carried out by all the other transmitters active over the network. Thus, the optimized design of the overall network involves a performance tradeoff among all active transmitters. Such a tradeoff is the subject of the present work. Specifically, the power-control and signal-shaping algorithms, which we propose, aim to maximize the information throughput conveyed by each link active over the network and are based on the modeling of the "*ad hoc*" network as a noncooperative strategic game. A game theoretic approach has been followed in several recent contributions dealing with power control in wireless networks [1], [4], [5], [18]. In addition, a game theory is also employed in [19] to solve the problem of the power allocation in single-user multiple-input multiple-output (MIMO) systems with imperfect channel estimation. However, all these works focus on scenarios characterized by either single-antenna terminals, where the spatial dimension of the system is fully neglected, or single user multiantenna terminals. Thus, the problem of the power allocation in MIMO systems, which is impaired by multiuser interference, still appears to be an open problem. On the contrary, in emerging next-generation "*ad hoc*" networks employing multiantenna transceivers, the spatial dimension of the overall system is crucial and must be explicitly taken into account in order to optimize the network throughput. The main result of this contribution is that, under suitable conditions, the multiantenna MAI channel game has a unique Nash equilibrium (NE) under both best-effort and "contracted QoS" access policies. This result leads to iterative fully scalable power-control and signal-shaping algorithms that are able to achieve the equilibrium point in a fully distributed and asynchronous way (see the Proposition 3). Specifically, the presented power-control and signal-shaping algorithms exhibit the following advantages over conventional centralized orthogonal access methods as time division multiple access (TDMA)/frequency division multiple access (FDMA)/code division multiple access (CDMA).

1) The proposed algorithms are fully scalable and may be implemented without any centralized controller.

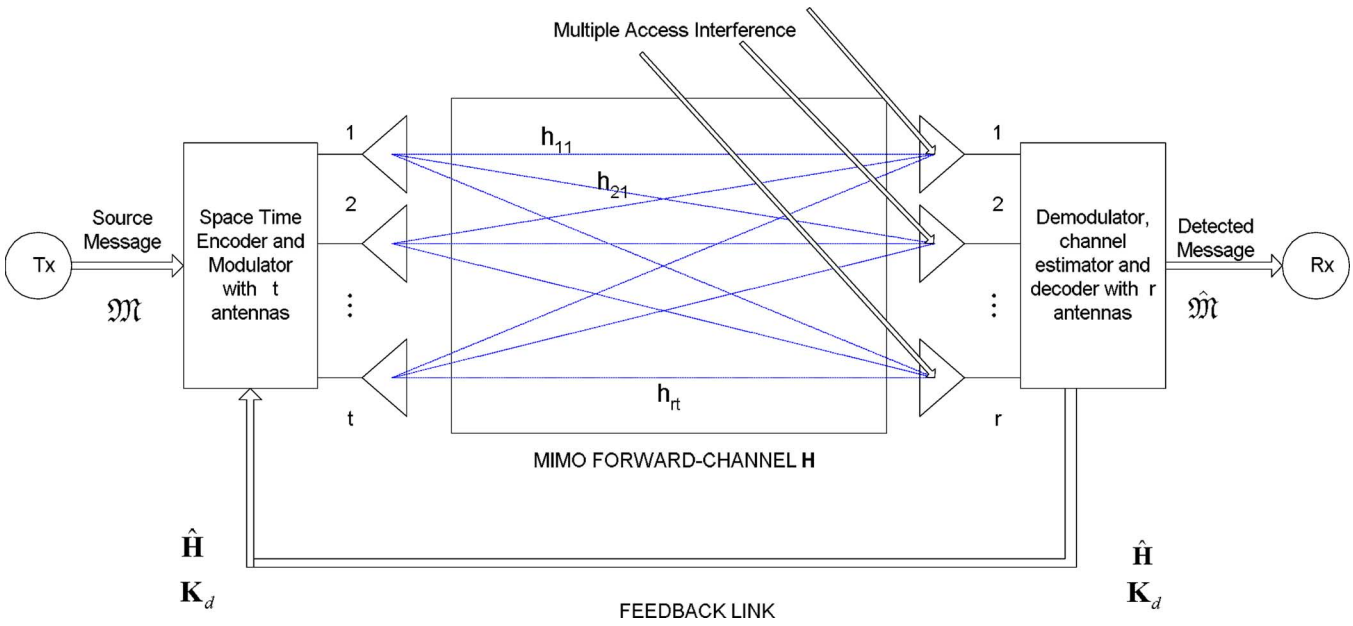

Fig. 1. Multiantenna system equipped with imperfect (forward) channel estimates $\hat{\mathbf{H}}$ and impaired by MAI with spatial covariance matrix $\mathbf{K}_{\mathrm{d}}$.

2) The proposed algorithms are competitively optimal, and then, they find an optimized balance between maximizing each user's own information throughput and minimizing its induced interference effect without completely avoiding it, as in [18], for a single-antenna scenario. For achieving this task, the spatial dimension of the underlying multiantenna channels is explicitly exploited.
3) The proposed algorithms allow to implement best-effort and "contracted QoS" access policies and may account for multiple QoS classes.
4) Several numerical results support the conclusion that the proposed distributed algorithms outperform conventional centralized ones (as TDMA/FDMA/CDMA) in terms of a conveyed information throughput, especially in networking scenarios affected by strong MAI.

B. Organization of the Work

The remainder of this paper is organized as follows. After giving the system model of Section II, the evaluation of the conveyed information throughput in MAI-affected environments is addressed in Section III. In Section IV, the optimized power allocation over the transmit antennas is presented for the simple case of a single transmit/receive pair impaired by "static" (e.g., not time varying) MAI. Thus, after shortly reviewing in Section V, the MAI model for the "*ad hoc*" networks proposed in [16], we formalize the concept of NE in Section VI, while in Section VII, we present iterative and fully decentralized algorithms for achieving the competitively optimal (e.g., maximum throughput) power allocation and signal shaping of all transmit/receive pairs active over the considered network. Analytical conditions for the convergence of the operating point of the overall network toward a stable state (e.g., the NE of the underlying game) are also provided in Section VII and proved in the final Appendices. The actual effectiveness of the proposed power-allocation and signal-shaping games is numerically tested in Section VIII, where some final conclusions are also drawn.

Before proceeding, we have a few words about the adopted notation. Capital letters indicate matrices, lower-case underlined symbols denote vectors, and characters overlined by an arrow $\vec{\ }$ denote block matrices and block vectors. Apexes *, $^{\mathrm{T}}$, † mean conjugation, transposition, and conjugate-transposition, respectively, while lower case letters will be used for scalar quantities. In addition, $\det[\mathbf{A}]$ and $\mathrm{Tra}[\mathbf{A}]$ mean determinant and trace of the matrix $\mathbf{A} \triangleq [\underline{\mathbf{a}}_1 \dots \underline{\mathbf{a}}_m]$, while $\mathrm{vect}(\mathbf{A})$ indicates the (block) vector obtained by the ordered stacking of the columns of $\mathbf{A}$. Finally, $\mathbf{I}_m$ is the $(m \times m)$ identity matrix, $\|\mathbf{A}\|_E$ is the Euclidean norm of the matrix $\mathbf{A}$ [6], $\mathbf{A} \otimes \mathbf{B}$ is the Kronecker product of matrix $\mathbf{A}$ by matrix $\mathbf{B}$ (see [6]), $\underline{\mathbf{0}}_m$ is the m-dimensional zero vector, lg denotes natural logarithm, and $\delta(m,n)$ is the Kroenecker delta.

II. System Modeling

In the application scenario, we consider models emerging wireless "*ad hoc*" networks [9], where a (large) number of uncoordinated transmit–receive nodes simultaneously attempt to communicate over a limited-size hot-spot cell and then give rise to MAI as in the scenario proposed in the framework of the Wireless 8O2.16 Multi-antenna mEsh Networks (WOMEN), where the lower level of communication between nodes is supposed to be in *ad hoc* mode [23]. The (complex base-band equivalent) point-to-point radio channel linking a transmitter node Tx to the corresponding receiving node Rx is sketched in Fig. 1. Simply stated, it is composed by a transmit unit equipped with $t \geq 1$ antennas communicating to a receive unit equipped with $r \geq 1$ antennas via a MIMO radio channel impaired by both slowly time-varying Rayleigh flat fading[1] and additive

[1]The assumption of flat fading is met when the RF bandwidth B_{w} of the signal radiated by each transmit antenna does not exceed the coherence bandwidth B_{c} of the MIMO forward channel of Fig. 1 [2], [10].

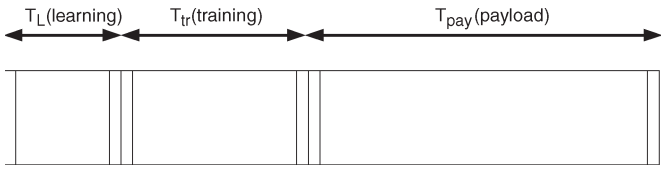

Fig. 2. Packet structure ($T \triangleq T_{\rm L} + T_{\rm tr} + T_{\rm pay}$).

MAI induced by adjacent transmit nodes active over the same hot-spot cell. The path gain h_{ji} from the transmit antenna i to the receive one j may be modeled as a complex zero-mean unit-variance proper complex random variable (r.v.) [2], [3], [11], and for sufficiently spaced apart antennas, overall path gains $\{h_{ji} \in \mathbb{C}^1, 1 \leq j \leq r, 1 \leq i \leq t\}$ may be considered mutually uncorrelated. Furthermore, for low-mobility applications such as those serving nomadic users over hot-spot cells, the path gains $\{h_{ji}\}$ may be also assumed time invariant over $T \geq 1$ signaling periods, after which, they change to new statistically independent values held for another T signaling periods, and so on. The resulting "block-fading" model well captures the main features of several frequency-hopping or packet-based interleaved 4G systems, where each transmitted packet is detected independently of any other [2], [3], [11], [16]. About the MAI affecting the link of Fig. 1, its statistics mainly depend on the network topology [2], [3], [11], and in the application scenario considered here, it is reasonable to assume that this topology remains constant over (at least) an overall packet [16]. However, since both path gains $\{h_{ji}\}$ and MAI statistics may change from a packet to another, we assume that Tx and Rx in Fig. 1 are not aware of them at the beginning of each transmitted packet. Hence, according to Fig. 2, we assume that the coded and modulated streams radiated by the transmit antennas are split into packets composed by $T \geq 1$ slots, where the first $T_{\rm L} \geq 0$ slots are used by the receiver for learning the MAI statistics (see Section II-A), the second $T_{\rm tr} \geq 0$ slots are employed for estimating the path gains $\{h_{ji}\}$ of the forward MIMO channel (see Section II-B), and the last $T_{\rm pay} \triangleq T - T_{\rm tr} - T_{\rm L}$ slots convey payload data (see Section II-C).

A. Learning Phase

During the learning phase (see Fig. 2), no signals are radiated by the transmitter of Fig. 1 to allow the corresponding receiver to learn the statistics of the impairing MAI. Specifically, the r-dimensional (complex column) vector $\underline{\dot{\mathbf{y}}}(n) \triangleq [\dot{y}_1(n) \ldots \dot{y}_r(n)]^{\rm T}$ collecting the outputs of the r receive antennas over the nth slot of the learning phase may be modeled as [17]

$$\underline{\dot{\mathbf{y}}}(n) \triangleq \underline{\dot{\mathbf{d}}}(n) \equiv \underline{\dot{\mathbf{v}}}(n) + \underline{\dot{\mathbf{w}}}(n), \qquad 1 \leq n \leq T_{\rm L} \tag{1}$$

where $\underline{\dot{\mathbf{y}}}(n)$ is the superposition of two mutually independent components $\underline{\dot{\mathbf{w}}}(n) \triangleq [\dot{w}_1(n) \ldots \dot{w}_r(n)]^{\rm T}$ and $\underline{\dot{\mathbf{v}}}(n) \triangleq [\dot{v}_1(n) \ldots \dot{v}_r(n)]^{\rm T}$. The first component accounts for the receiver thermal noise, so that $\{\underline{\dot{\mathbf{w}}}(n) \in \mathbb{C}^r, 1 \leq n \leq T_{\rm L}\}$ may be modeled as a zero-mean proper complex spatially and temporally white Gaussian sequence with covariance matrix equal to

$$E\left\{\underline{\dot{\mathbf{w}}}(n)\left(\underline{\dot{\mathbf{w}}}(m)\right)^{\dagger}\right\} = \mathcal{N}_0 \mathbf{I}_r \delta(m,n) \tag{2}$$

where $\mathcal{N}_0$ (watt/Hz) is the level of the receiver's thermal noise. The component $\{\underline{\dot{\mathbf{v}}}(n)\}$ in (1) accounts for the MAI induced by multiple colocated transmit nodes active over the same hot-spot cell, and then, it may be adequate to model $\{\underline{\dot{\mathbf{v}}}(n) \in \mathbb{C}^r\}$ as a zero-mean temporally white spatially colored proper Gaussian sequence [12], [16] whose covariance matrix

$$\mathbf{K}_{\rm v} \triangleq E\left\{\underline{\dot{\mathbf{v}}}(n)\left(\underline{\dot{\mathbf{v}}}(n)\right)^{\dagger}\right\} \equiv \begin{bmatrix} c_{11} & \ldots & c_{1r} \\ c_{12}^* & \ldots & c_{2r} \\ \vdots & \vdots & \vdots \\ c_{1r}^* & \ldots & c_{rr} \end{bmatrix} \tag{3}$$

remains constant over time intervals at least equal to the duration of an overall packet (see Fig. 2). However, $\mathbf{K}_{\rm v}$ may change from a packet to another, so that it is reasonable to assume that both the transmit and receive nodes in Fig. 1 are not aware of the covariance matrix of the overall disturbance

$$\mathbf{K}_{\rm d} \triangleq E\left\{\underline{\dot{\mathbf{y}}}(n)\left(\underline{\dot{\mathbf{y}}}(n)\right)^{\dagger}\right\} \equiv \mathbf{K}_{\rm v} + \mathcal{N}_0 \mathbf{I}_r \tag{4}$$

at the beginning of each transmitted packet. During the learning phase, the received signal $\underline{\dot{\mathbf{y}}}(n)$ in (1) equates the MAI $\underline{\dot{\mathbf{d}}}(n)$, and the law of large numbers guarantees that an unbiased and consistent (e.g, asymptotically exact) estimate $\overset{\vee}{\mathbf{K}}_{\rm d}$ of the (*a priori*) unknown covariance matrix $\mathbf{K}_{\rm d}$ may be evaluated via the following sample average:

$$\overset{\vee}{\mathbf{K}}_{\rm d} = \frac{1}{T_{\rm L}} \sum_{n=1}^{T_{\rm L}} \underline{\dot{\mathbf{y}}}(n)\left(\underline{\dot{\mathbf{y}}}(n)\right)^{\dagger}. \tag{5}$$

As already pointed out in [11], the effects of (possible) mismatches between the actual $\mathbf{K}_{\rm d}$ and its estimate $\overset{\vee}{\mathbf{K}}_{\rm d}$ are not so critical, so that in the following, we directly assume that $\overset{\vee}{\mathbf{K}}_{\rm d} = \mathbf{K}_{\rm d}$. However, this assumption will be relaxed in Section VIII-B, where the effects of possible mismatches between actual $\mathbf{K}_{\rm d}$ and the estimated one $\overset{\vee}{\mathbf{K}}_{\rm d}$ are numerically evaluated.

B. Training Phase

During the training phase, the Tx transmit node of Fig. 1 is able to perform the optimized shaping of the deterministic pilot streams $\{\widetilde{x}_i(n) \in \mathbb{C}^1, T_{\rm L}+1 \leq n \leq T_{\rm L}+T_{\rm tr}\}$, $1 \leq i \leq t$, to be used for estimating the (*a priori* unknown) $(r \times t)$ path gains $\{h_{ji}\}$ of the MIMO forward channel of Fig. 1. In particular, the (sampled) signals $\{\widetilde{y}_j(n) \in \mathbb{C}^1, T_{\rm L}+1 \leq n \leq T_{\rm L}+T_{\rm tr}, 1 \leq j \leq r\}$ measured at the output of jth receive antenna during the training phase may be modeled as [17]

$$\widetilde{y}_j(n) = \frac{1}{\sqrt{t}} \sum_{i=1}^{t} h_{ji}\widetilde{x}_i(n) + \widetilde{d}_j(n) \qquad T_{\rm L}+1 \leq n \leq T_{\rm L}+T_{\rm tr}, \qquad 1 \leq j \leq r \tag{6}$$

where the corresponding overall disturbance

$$\widetilde{d}_j(n) \triangleq \widetilde{v}_j(n) + \widetilde{w}_j(n),\ T_L + 1 \le n \le T_{\rm L} + T_{\rm tr},\ 1 \le j \le r \tag{7}$$

is independent from the path gains $\{h_{ji}\}$ and exhibits the same statistics previously reported in (4) for the learning phase. Thus, after assuming the (usual) power constraint [2]

$$\frac{1}{t}\sum_{i=1}^{t} \|\widetilde{x}_i(n)\|^2 \le \widetilde{P},\ T_{\rm L} + 1 \le n \le T_{\rm L} + T_{\rm tr} \tag{8}$$

on the average power $\widetilde{P}$ radiated by the transmit antennas over each slot of the training phase, the resulting signal to interference-plus-noise ratio (SINR) $\widetilde{\gamma}_j$ measured at the output of jth receive antenna equals [see (7) and (8)]

$$\widetilde{\gamma}_j = \widetilde{P}/(\mathcal{N}_0 + c_{jj}), \qquad 1 \le j \le r \tag{9}$$

where $\mathcal{N}_0 + c_{jj}$ is the jth diagonal entry of the MAI matrix $\mathbf{K}_{\rm d}$ in (4). Therefore, as in [2], the $T_{\rm tr} \times r$ (complex) samples gathered at the outputs of the r receive antennas during the overall training phase may be organized into the $(T_{\rm tr} \times r)$ observed matrix $\widetilde{\mathbf{Y}} \triangleq [\underline{\widetilde{y}}_1 \dots \underline{\widetilde{y}}_r]$ given by

$$\widetilde{\mathbf{Y}} = \frac{1}{\sqrt{t}}\widetilde{\mathbf{X}}\mathbf{H} + \widetilde{\mathbf{D}} \tag{10}$$

where $\widetilde{\mathbf{X}} \triangleq [\underline{\widetilde{x}}_1 \dots \underline{\widetilde{x}}_t]$ is the $(T_{\rm tr} \times t)$ matrix composed by the (deterministic) radiated pilot symbols, $\mathbf{H} \triangleq [\underline{\mathbf{h}}_1 \dots \underline{\mathbf{h}}_r]$ is the $(t \times r)$ complex matrix composed by the path gains $\{h_{ji}\}$ to be estimated, and the $(T_{\rm tr} \times r)$ matrix $\widetilde{\mathbf{D}} \triangleq [\underline{\widetilde{\mathbf{d}}}_1 \dots \underline{\widetilde{\mathbf{d}}}_r]$ collects the disturbance samples $\{\widetilde{d}_j(n)\}$ in (7) experienced during the training phase. Obviously, from (8), it follows that the pilot matrix $\widetilde{\mathbf{X}}$ in (10) must satisfy the following power constraint:

$$\mathrm{Tra}[\widetilde{\mathbf{X}}\widetilde{\mathbf{X}}^{\dagger}] \le tT_{\rm tr}\widetilde{P}. \tag{11}$$

As detailed in [11] and [14], the trained observations $\widetilde{\mathbf{Y}}$ in (10) are employed by the receive node of Fig. 1 for computing the minimum mean square error (mmse) matrix estimate $\hat{\mathbf{H}} \triangleq E\{\mathbf{H}|\widetilde{\mathbf{Y}}\}$ of the MIMO channel matrix $\mathbf{H}$. In turn, at step $n = T_{\rm L} + T_{\rm tr}$ (e.g., at the end of the training phase), this estimate $\hat{\mathbf{H}}$ is communicated back to the transmitter via the (ideal) feedback link of Fig. 1.

C. Some Consideration About the Optimized Training

A detailed analysis about the structure and performance of the estimator computing the set $\{\hat{h}_{ji} \triangleq E\{h_{ji}|\tilde{\mathbf{Y}}\}, 1 \le j \le r, 1 \le i \le t\}$ of the $(r \times t)$ mmse channel estimates of the MIMO forward channel $\mathbf{H}$ in (10) may be found in [11] and [14] so that thereinafter, we only summarize some basic results exploited in the next sections. In particular, in [11] and [14], it is proved that under the power constraint (11), the pilot matrix $\tilde{\mathbf{X}}$ minimizing the total average squared estimation error

$$\sigma^2_{\rm tot} \triangleq \sum_{j=1}^{r}\sum_{i=1}^{t} E\left\{\|\hat{h}_{ji} - h_{ji}\|^2\right\} \equiv \sum_{j=1}^{r}\sum_{i=1}^{t} E\left\{\|\varepsilon_{ji}\|^2\right\}$$

must satisfy the following relationship:

$$\mathbf{K}_{\rm d}^{-1} \otimes \tilde{\mathbf{X}}^{\dagger}\tilde{\mathbf{X}} = a\mathbf{I}_{\rm rt} \tag{11.1}$$

with

$$a \triangleq \frac{T_{\rm tr}\tilde{P}}{r}\mathrm{Tra}\left[\mathbf{K}_{\rm d}^{-1}\right]. \tag{11.2}$$

Furthermore, when $\tilde{\mathbf{X}}$ meets (11.1), the resulting mmse channel estimator errors $\{\varepsilon_{ji} \triangleq \hat{h}_{ji} - h_{ji}, 1 \le j \le r, 1 \le i \le t\}$ are mutually uncorrelated, zero mean, proper complex equidistributed Gaussian r.v.s sharing the following variance [11], [14]:

$$\sigma^2_{\varepsilon} \triangleq E\left\{\|\varepsilon_{ji}\|^2\right\} \equiv E\left\{\|\hat{h}_{ji} - h_{ji}\|^2\right\} = (1 + a/t)^{-1}. \tag{11.3}$$

In the following, we assume that (11.1) is satisfied, and then, we proceed to evaluate the performance of the considered system of Fig. 1 on the basis of (11.3). Additional details about the overall topic of the optimized mmse MIMO channel estimates as well as considerations about the system sensitivity to a noisy (e.g., no ideal) feedback link may be found in [14].

D. Payload Phase

On the basis of the available $\mathbf{K}_{\rm d}$ and $\hat{\mathbf{H}}$ matrices and actual packet $\mathfrak{M}$ to be transmitted, the transmit node of Fig. 1 suitably shapes the signal streams $\{\phi_i(n) \in \mathbb{C}^1, T_{\rm L} + T_{\rm tr} + 1 \le n \le T\}$, $1 \le i \le t$, to be radiated during the payload phase. The corresponding (sampled) signals $\{y_j(n) \in \mathbb{C}^1, T_{\rm L} + T_{\rm tr} + 1 \le n \le T\}$, $1 \le j \le r$, measured at the outputs of the receive antennas, may be modeled as [17]

$$y_j(n) = \frac{1}{\sqrt{t}}\sum_{i=1}^{t} h_{ji}\phi_i(n) + d_j(n) \qquad T_{\rm L} + T_{\rm tr} + 1 \le n \le T, \qquad 1 \le j \le r \tag{12}$$

where the sequences $d_j(n) \triangleq v_j(n) + w_j(n)$, $1 \le j \le r$ account for the overall disturbance (e.g., MAI plus thermal noise) experienced during the payload phase. They still exhibit the same statistics previously detailed in (4) and may also be assumed independent from both path gains $\{h_{ji}\}$ and payload streams $\{\phi_i\}$ [17]. Therefore, after assuming that the transmitted streams meet the (usual) power constraint [2]

$$\frac{1}{t}\sum_{i=1}^{t} E\left\{\|\phi_i(n)\|^2\right\} \le P, \quad T_{\rm L} + T_{\rm tr} + 1 \le n \le T \tag{13}$$

the resulting SINR γ_j measured at the output of the jth receive antenna during the payload phase equals[2] [see (12) and (13)]

$$\gamma_j = P/(\mathcal{N}_0 + c_{jj}), \qquad 1 \le j \le r. \tag{14}$$

Furthermore, from (12), we also deduce that the $(r \times 1)$ column vector $\underline{\mathbf{y}}(n) \triangleq [y_1(n) \dots y_r(n)]^{\mathrm{T}}$ collecting the outputs of the r receive antennas over the nth payload slot is linked to the $(t \times 1)$ column vector $\underline{\boldsymbol{\phi}}(n) \triangleq [\phi_1(n) \dots \phi_t(n)]^{\mathrm{T}}$ of the corresponding signals radiated by the transmit node as in

$$\underline{\mathbf{y}}(n) = \frac{1}{\sqrt{t}}\mathbf{H}^{\mathrm{T}}\underline{\boldsymbol{\phi}}(n) + \underline{\mathbf{d}}(n), \quad T_{\mathrm{L}} + T_{\mathrm{tr}} + 1 \le n \le T \tag{15}$$

where $\{\underline{\mathbf{d}}(n) \triangleq [d_1(n) \dots d_r(n)]^{\mathrm{T}}, T_{\mathrm{L}} + T_{\mathrm{tr}} + 1 \le n \le T\}$ is the (temporally white) Gaussian sequence of disturbances with spatial covariance matrix still given by $\mathbf{K}_{\mathrm{d}}$ in (4). Furthermore, directly from (13), it follows that the $(t \times t)$ spatial covariance matrix $\mathbf{R}_{\boldsymbol{\phi}} \triangleq E\{\underline{\boldsymbol{\phi}}(n)\underline{\boldsymbol{\phi}}(n)^{\dagger}\}$ of the t-dimensional signal vector radiated during each slot must meet the following power constraint:

$$\mathrm{Tra}[\mathbf{R}_{\boldsymbol{\phi}}] \equiv E\left\{\underline{\boldsymbol{\phi}}(n)^{\dagger}\underline{\boldsymbol{\phi}}(n)\right\} \le tP, \quad T_{\mathrm{L}} + T_{\mathrm{tr}} + 1 \le n \le T. \tag{16}$$

Finally, after stacking the T_{pay} observed vectors in (15) into the corresponding $(T_{\mathrm{pay}}r \times 1)$ block vector $\overrightarrow{\underline{\mathbf{y}}} \triangleq [\underline{\mathbf{y}}^{\mathrm{T}}(T_{\mathrm{L}} + T_{\mathrm{tr}} + 1) \dots \underline{\mathbf{y}}^{\mathrm{T}}(T)]^{\mathrm{T}}$, we may compact the T_{pay} relationships (15) into the following one:

$$\overrightarrow{\underline{\mathbf{Y}}} = \frac{1}{\sqrt{t}}\left[\mathbf{I}_{T_{\mathrm{pay}}} \otimes \mathbf{H}\right]^{\mathrm{T}}\overrightarrow{\underline{\boldsymbol{\phi}}} + \overrightarrow{\underline{\mathbf{d}}} \tag{17}$$

where the (block) covariance matrix of the corresponding disturbance (block) vector in (17) $\overrightarrow{\underline{\mathbf{d}}} \triangleq [\underline{\mathbf{d}}^{\mathrm{T}}(T_{\mathrm{L}} + T_{\mathrm{tr}} + 1) \dots \underline{\mathbf{d}}^{\mathrm{T}}(T)]^{\mathrm{T}}$ equals,

$$E\left\{\overrightarrow{\underline{\mathbf{d}}}(\overrightarrow{\underline{\mathbf{d}}})^{\dagger}\right\} = \mathbf{I}_{T_{\mathrm{pay}}} \otimes \mathbf{K}_{\mathrm{d}} \tag{18}$$

while the squared norm of the block vector $\overrightarrow{\underline{\boldsymbol{\phi}}} \triangleq [\underline{\boldsymbol{\phi}}^{\mathrm{T}}(T_{\mathrm{L}} + T_{\mathrm{tr}} + 1) \dots \underline{\boldsymbol{\phi}}^{\mathrm{T}}(T)]^{\mathrm{T}}$ of the random signals transmitted during the payload phase is constrained as in [see (16)]

$$E\left\{\overrightarrow{\underline{\boldsymbol{\phi}}}^{\dagger}\overrightarrow{\underline{\boldsymbol{\phi}}}\right\} \le T_{\mathrm{pay}}tP. \tag{19}$$

III. Conveyed Information Throughput in the Presence of Channel-Estimation Errors and Spatially Colored MAI

The block-fading model introduced in Section II for the MIMO channel of Fig. 1 guarantees that this last one is information stable [8] so that the corresponding Shannon's capacity C (nats/slot) fixes the maximum information throughput conveyable in a reliable way during the payload phase [7]. Following quite standard approaches [7], the capacity C of the MIMO channel (17) can be expressed as

$$C = E\left\{C(\hat{\mathbf{H}})\right\} \equiv \int C(\hat{\mathbf{H}})p(\hat{\mathbf{H}})d\hat{\mathbf{H}}, \qquad \text{(nats/slot)} \tag{20}$$

where $p(\hat{\mathbf{H}}) = (1/\pi(1-\sigma_{\varepsilon}^2))^{\mathrm{rt}} \exp\{-(1/(1-\sigma_{\varepsilon}^2))\mathrm{Tra}[\hat{\mathbf{H}}^{\dagger}\hat{\mathbf{H}}]\}$ is the Gaussian probability density function (pdf) of the above introduced channel estimates $\hat{\mathbf{H}}$ [11], and the random variable

$$C(\hat{\mathbf{H}}) \triangleq \sup_{\overrightarrow{\underline{\boldsymbol{\phi}}}: E\{\overrightarrow{\underline{\boldsymbol{\phi}}}^{\dagger}\overrightarrow{\underline{\boldsymbol{\phi}}}\} \le tT_{\mathrm{pay}}P} \frac{1}{T_{\mathrm{pay}}} I\left(\overrightarrow{\underline{\mathbf{y}}}; \overrightarrow{\underline{\boldsymbol{\phi}}}|\hat{\mathbf{H}}\right), \text{ (nats/slot)} \tag{21}$$

is Shannon's capacity of the MIMO channel (17) conditioned on the realization $\hat{\mathbf{H}}$ of the channel estimates that are actually available at both the transmitter and receiver of Fig. 1. Finally, $I(\cdot;\cdot|\cdot)$ in (21) denotes the mutual information conveyed by the MIMO channel (17) during the payload phase [7]. Unfortunately, barring the limit cases of perfect channel state information (PCSI) and no CSI [2], [10], the pdf of the input signals $\overrightarrow{\underline{\boldsymbol{\phi}}}$ achieving the supremum in (21) is currently unknown, even in the simplest case of spatially white MAI [10]. However, it is known that Gaussian distributed input signals achieve the supremum in (21) both when the condition of PCSI is approached [2], as well as for imperfect channel estimates when the length T_{pay} of the payload phase (largely) exceeds the number t of transmit antennas (see, for example, [14] and [20] about this asymptotic result). Therefore, motived by the above considerations, in the following, we focus on the evaluation of (21) for Gaussian distributed input signals. In this case, the T_{pay} components $\{\underline{\boldsymbol{\phi}}(n) \in \mathbb{C}^t, T_{\mathrm{L}} + T_{\mathrm{tr}} + 1 \le n \le T\}$ in (15) of the overall signal vector $\overrightarrow{\underline{\boldsymbol{\phi}}}$ in (17) are uncorrelated zero-mean proper complex Gaussian vectors with correlation matrix $\mathbf{R}_{\boldsymbol{\phi}}$ meeting (16). The corresponding information throughput

$$\mathbb{T}_{\mathrm{G}}(\hat{\mathbf{H}}) \triangleq \frac{1}{T_{\mathrm{pay}}} \sup_{\mathrm{Tra}[\mathbf{R}_{\boldsymbol{\phi}}] \le Pt} I\left(\overrightarrow{\underline{\mathbf{y}}}; \overrightarrow{\underline{\boldsymbol{\phi}}}|\hat{\mathbf{H}}\right), \text{ (nats/slot)} \tag{22}$$

conveyed by the MIMO channel (17) for Gaussian input signals generally falls below the Shannon's Capacity $C(\hat{\mathbf{H}})$ in (21) so that we have $\mathbb{T}_{\mathrm{G}}(\hat{\mathbf{H}}) \le C(\hat{\mathbf{H}})$. However, the above inequality is satisfied as equality when at least one of the above cited two operating conditions (e.g., CSI or large T_{pay}) is met [14], [20]. Therefore, for the evaluation of $\mathbb{T}_{\mathrm{G}}(\hat{\mathbf{H}})$ in (22), we remark that, in general, the conditional mutual information $I(\overrightarrow{\underline{\mathbf{y}}}; \overrightarrow{\underline{\boldsymbol{\phi}}}|\hat{\mathbf{H}})$ in (22) resists closed-form computation [10]. However, in [11] and [14], the following result is presented.

Proposition 1: Let us assume that the spatial correlation matrix $\mathbf{R}_{\boldsymbol{\phi}}$ in (16) of the payload streams radiated by the transmit antennas of Fig. 1 is assigned. Thus, the resulting conditional mutual information $I(\overrightarrow{\underline{\mathbf{y}}}; \overrightarrow{\underline{\boldsymbol{\phi}}}|\hat{\mathbf{H}})$ in (21), which is supported by

[2]We point out that our model explicitly accounts for the different power levels $\widetilde{P}$ and P possibly radiated by transmit antennas during the training and payload phases, respectively.

the MIMO channel (17) for Gaussian input signals, admits the following closed-form expression (see [11] and [14]):

$$I\left(\underline{\overrightarrow{\mathbf{y}}};\underline{\overrightarrow{\phi}}|\hat{\mathbf{H}}\right) = T_{\rm pay}\lg\det\left(\mathbf{I}_r+\frac{1}{t}\mathbf{K}_{\rm d}^{-1/2}\hat{\mathbf{H}}^{\rm T}\mathbf{R}_{\boldsymbol{\phi}}\hat{\mathbf{H}}^{*}\mathbf{K}_{\rm d}^{-1/2}+\sigma_{\varepsilon}^2P\mathbf{K}_{\rm d}^{-1}\right) - \lg\det\left(\mathbf{I}_{\rm rt}+\frac{\sigma_{\varepsilon}^2T_{\rm pay}}{t}\left(\mathbf{K}_{\rm d}^{-1}\right)^{*}\otimes\mathbf{R}_{\boldsymbol{\phi}}\right) \tag{23}$$

when at least one of the following conditions is met:

$$\text{both } T_{\rm pay} \text{ and } t \text{ are large} \tag{24}$$

$$\hat{\mathbf{H}} \text{ approaches } \mathbf{H} \tag{25}$$

$$\text{all SINRs } \gamma_j,\ 1\le j\le r \text{ in } (14) \text{ vanish.} \tag{26}$$

A detailed proof about the above Proposition may be found in [14] and, for the sake of brevity, it is omitted here.

IV. Optimized Power Allocation and Signal Shaping in the Presence of Colored MAI and Channel-Estimation Errors

Therefore, according to (22), we must proceed to carry out the power-constrained maximization[3] of the conditional throughput (23). For this purpose, let us indicate as

$$\mathbf{K}_{\rm d}=\mathbf{U}_{\rm d}\boldsymbol{\Lambda}_{\rm d}\mathbf{U}_{\rm d}^{\dagger} \tag{27}$$

the singular value decomposition (SVD) of the MAI spatial covariance matrix $\mathbf{K}_{\rm d}$, where

$$\boldsymbol{\Lambda}_{\rm d}\triangleq\operatorname{diag}\{\mu_1,\ldots,\mu_r\} \tag{28}$$

is the corresponding $(r\times r)$ diagonal matrix of the magnitude-ordered singular values of $\mathbf{K}_{\rm d}$. Thus, after introducing the $(t\times r)$ matrix

$$\mathbf{A}\triangleq\hat{\mathbf{H}}^{*}\mathbf{K}_{\rm d}^{-1/2}\mathbf{U}_{\rm d} \tag{29}$$

accounting for the combined effects of the imperfect channel estimate $\hat{\mathbf{H}}$ and spatial MAI $\mathbf{K}_{\rm d}$, let us denote as

$$\mathbf{A}=\mathbf{U}_A\mathbf{D}_A\mathbf{V}_A^{\dagger} \tag{30}$$

the corresponding SVD, where $\mathbf{U}_A$ and $\mathbf{V}_A$ are unitary matrices, while

$$\mathbf{D}_A\triangleq\operatorname{diag}\{k_1,\ldots,k_s,\underline{\mathbf{0}}_{t-s}\} \tag{31}$$

[3]It is important to underline that the steps, which are performed to derive the algorithm for power allocation, are the same as the well-known water-filling one (in fact, when we consider $\mathbf{K}_{\rm d}=\mathcal{N}_0\mathbf{I}_r$ and $\sigma_{\varepsilon}^2=0$, the algorithm reduces itself to the standard water-filling one. However, the presence of additional elements such as imperfect channel estimates and spatially colored interference gives rise to different expression to be maximized (23), and the conditions to allocate power become different with respect to the standard water-filling approach (see [22]).

is the $(t\times r)$ diagonal matrix collecting the $s\triangleq\min\{r,t\}$ magnitude-ordered singular values $k_1\ge k_2\ge\ldots\ge k_s>0$ of matrix $\mathbf{A}$. Finally, for future convenience, let us also introduce the following dummy positions:

$$\alpha_m\triangleq\frac{\mu_m k_m^2}{t(\mu_m+P\sigma_{\varepsilon}^2)},\ 1\le m\le s;\quad \beta_l\triangleq\frac{\sigma_{\varepsilon}^2T_{\rm pay}}{t\mu_l},\ 1\le l\le r. \tag{32}$$

It can be proven (see [11] and [14]) that the application of the Kuhn–Tucker conditions [7] allows us to evaluate the optimized transmit powers $\{P^{\star}(m),1\le m\le t\}$ achieving the constrained supremum in (22), as detailed by the following Proposition 2.

Proposition 2: Let us assume that at least one of the operating conditions listed in (24)–(26) is fulfilled. Thus, for $m=s+1,\ldots,t$, the powers $\{P^{\star}(m)\}$ achieving the supremum in (22) vanish, while for $m=1,\ldots,s$, they must be computed according to the following two relationships:

$$P^{\star}(m)=0,\ \text{when } k_m^2\le\left(1+\frac{\sigma_{\varepsilon}^2P}{\mu_m}\right)\left(\frac{t}{\rho}+\sigma_{\varepsilon}^2\text{Tra}\left[\mathbf{K}_{\rm d}^{-1}\right]\right) \tag{33}$$

$$P^{\star}(m)=\frac{1}{2\beta_{\min}}\times\left\{\beta_{\min}L-1+\sqrt{\{\beta_{\min}L\}^2+4\beta_{\min}\left(\rho-\frac{1}{\alpha_m}-\frac{r\rho\beta_{\min}}{\alpha_m T_{\rm pay}}\right)}\right\}$$
$$\text{when } k_m^2>\left(1+\frac{\sigma_{\varepsilon}^2P}{\mu_m}\right)\left(\frac{t}{\rho}+\sigma_{\varepsilon}^2\text{Tra}\left[\mathbf{K}_{\rm d}^{-1}\right]\right) \tag{34}$$

where $\beta_{\min}\triangleq\min\{\beta_l,l=1,\ldots,r\}$, and $L\triangleq(1-(r/T_{\rm pay}))\rho-(1/\alpha_m)$. Furthermore, the nonnegative scalar parameter ρ in (33), (34) is set so to satisfy the following power constraint [see (13)]:

$$\sum_{m\in\mathfrak{I}(\rho)}P^{\star}(m)\le Pt \tag{35}$$

where

$$\mathfrak{I}(\rho)\triangleq\left\{m=1,\ldots,s:k_m^2>\left(1+\frac{\sigma_{\varepsilon}^2P}{\mu_m}\right)\times\left(\frac{t}{\rho}+\sigma_{\varepsilon}^2\text{Tra}\left[\mathbf{K}_{\rm d}^{-1}\right]\right)\right\} \tag{36}$$

is the (ρ-dependent) set of m-indexes fulfilling the inequality in (34). Finally, the corresponding optimized spatial correlation

matrix $\mathbf{R}_{\boldsymbol{\phi}}(\mathrm{opt})$ for the radiated signals is aligned along the right eigenvectors of the matrix $\mathbf{A}$ in (29) as in

$$\mathbf{R}_{\boldsymbol{\phi}}(\mathrm{opt}) = \mathbf{U}_A \mathrm{diag}\left\{P^{\star}(1), \ldots P^{\star}(s), \underline{\mathbf{0}}_{t-s}\right\} \mathbf{U}_A^{\dagger} \quad (37)$$

so that the resulting maximized information throughput in (22) admits the following (simple) closed-form expression (see [11] and [14]):

$$\mathbb{T}_{\mathrm{G}}(\hat{\mathbf{H}}) = \sum_{m=1}^{r} \lg\left(1 + \frac{\sigma_{\varepsilon}^2 P}{\mu_m}\right) + \sum_{m=1}^{s} \left[\lg\left(1 + \alpha_m P^{\star}(m)\right) - \frac{1}{T_{\mathrm{pay}}} \sum_{l=1}^{r} \lg\left(1 + \beta_l P^{\star}(m)\right)\right]. \quad (38)$$

V. Topology-Based MAI Model for MultiAntenna *ad hoc* Networks

To test the actual effectiveness of the proposed power-allocation and signal-shaping algorithms, we consider the application scenario sketched in Fig. 3 that may be considered adequate to capture the key features of the spatial MAI impairing emerging multiantenna "*ad hoc*" networks [9], [16]. Specifically, the considered network is composed by n^* noncooperative, mutually interfering, point-to-point links $T_{\mathrm{xf}} \rightarrow R_{\mathrm{xf}}$, $1 \leq f \leq n^*$, so that the overall (vector) signal received by the gth receive node R_{xg} is the superposition of the desired signal generated by T_{xg} together with the $(n^* - 1)$ interfering signals radiated by all other transmit nodes $\{T_{\mathrm{xf}}, f \neq g\}$. Each transmit node T_{xf} is assumed to be equipped with t_f, $1 \leq f \leq n^*$ transmit antennas, while r_f, $1 \leq f \leq n^*$ indicates the number of antennas located at the corresponding receive node R_{xf}. Thus, after indicating as $l(f,g)$ the length of the link $T_{\mathrm{xf}} \rightarrow R_{\mathrm{xf}}$, the r_g-dimensional disturbance $\underline{\mathbf{d}}^{(g)}(n)$ in (15) received by R_{xg} during the nth slot of the payload phase may be adequately modeled as [16][4]

$$\underline{\mathbf{d}}^{(g)}(n) = \sum_{f=1, f\neq g}^{N} \sqrt{\left(\frac{l(g,g)}{l(f,g)}\right)^4} \frac{1}{\sqrt{t_g}} \chi(f,g) \times \mathbf{H}^{\mathrm{T}}(f,g) \underline{\boldsymbol{\phi}}^{(f)}(n) + \underline{\mathbf{w}}^{(g)}(n) \quad (39)$$

where $\underline{\mathbf{w}}^{(g)}(n)$ accounts for the thermal noise present in R_{xg}, $\underline{\boldsymbol{\phi}}^{(f)}(n)$ is the t_f-dimensional (Gaussian) signal radiated by T_{xf}, $\chi(f,g)$ accounts for the shadowing effects[5] possibly present on the link $T_{\mathrm{xf}} \rightarrow R_{\mathrm{xg}}$, and the $(t_f \times r_g)$ matrix $\mathbf{H}(f,g)$ describes Ricean-distributed fast fading affecting the link $T_{\mathrm{xf}} \rightarrow R_{\mathrm{xg}}$. Specifically, according to the fast-fading spatial interference model recently developed in [16], the channel matrix $\mathbf{H}(f,g)$ in (39) may be modeled as [16]

$$\mathbf{H}(f,g) \equiv \sqrt{\frac{k(f,g)}{1+k(f,g)}} \mathbf{H}^{(\mathrm{sp})}(f,g) + \sqrt{\frac{1}{1+k(f,g)}} \mathbf{H}^{(\mathrm{sc})}(f,g), \qquad 1 \leq f,g \leq n^* \quad (40)$$

where $k(f,g) \in [0, +\infty)$ is the Ricean factor of the link $T_{\mathrm{xf}} \rightarrow R_{\mathrm{xg}}$, while the elements of the $(t_f \times r_g)$ matrix $\mathbf{H}^{(\mathrm{sc})}(f,g)$ are mutually independent zero-mean unit-variance proper Gaussian r.v.s. accounting for the scattered propagation component of the link $T_{\mathrm{xf}} \rightarrow R_{\mathrm{xg}}$. Furthermore, according to [16], the $(t_f \times r_g)$ specular propagation component matrix $\mathbf{H}^{(\mathrm{sp})}(f,g)$ of the link $T_{\mathrm{xf}} \rightarrow R_{\mathrm{xg}}$ may be evaluated as

$$\mathbf{H}^{(\mathrm{sp})}(f,g) \equiv \underline{\mathbf{a}}(f,g) \underline{\mathbf{b}}^{\mathrm{T}}(f,g), \qquad 1 \leq f,g \leq n^* \quad (41)$$

where $\underline{\mathbf{a}}(f,g)$ and $\underline{\mathbf{b}}(f,g)$ are the $(t_f \times 1)$ and $(r_g \times 1)$ column vectors describing the specular array responses at R_{xg} and T_{xf}, respectively [16]. In particular, when regularly spaced linear arrays with isotropic elements are employed at R_{xg} and T_{xf}, the above vectors may be directly evaluated as in [16]

$$\underline{\mathbf{a}}(f,g) = \left[1, \exp\left(j2\pi\nu \cos\left(\theta_{\mathrm{a}}(f,g)\right)\right), \ldots \exp\left(j2\pi\nu(r_f - 1)\cos\left(\theta_{\mathrm{a}}(f,g)\right)\right)\right]^{\mathrm{T}} \quad (42)$$

$$\underline{\mathbf{b}}(f,g) = \left[1, \exp\left(j2\pi\nu \cos\left(\theta_{\mathrm{d}}(f,g)\right)\right), \ldots \exp\left(j2\pi\nu(r_g - 1)\cos\left(\theta_{\mathrm{d}}(f,g)\right)\right)\right]^{\mathrm{T}} \quad (43)$$

where $\theta_{\mathrm{a}}(f,g)$ and $\theta_{\mathrm{d}}(f,g)$ are the arrival and departure angles for the link $T_{\mathrm{xf}} \rightarrow R_{\mathrm{xg}}$ (see Fig. 3), while ν is the antenna spacing in multiple of RF radiated wavelength.[6] Thus, on the basis of the model (40), (41), the resulting MAI covariance matrix $\mathbf{K}_{\mathrm{d}}^{(g)}$ measured by R_{xg} assumes the following form:

$$\begin{aligned}\mathbf{K}_{\mathrm{d}}^{(g)} &\triangleq E\left\{\underline{\mathbf{d}}^{(g)}(n)\left(\underline{\mathbf{d}}^{(g)}(n)\right)^{\dagger}\right\} \\ &\equiv \left\{\mathcal{N}_0 + \sum_{\substack{f=1 \\ f\neq g}}^{n^*} \left(\frac{l(g,g)}{l(f,g)}\right)^4 \frac{\chi^2(f,g)}{1+k(f,g)} P^{(f)}\right\} \mathbf{I}_{r_g} \\ &\quad + \left\{\sum_{\substack{f=1 \\ f\neq g}}^{n^*} \left(\frac{l(g,g)}{l(f,g)}\right)^4 \frac{k(f,g)}{1+k(f,g)} \frac{\chi^2(f,g)}{t_f} \times \underline{\mathbf{a}}(f,g)\underline{\mathbf{b}}^{\mathrm{T}}(f,g)\mathbf{R}_{\boldsymbol{\phi}}^{(f)}\underline{\mathbf{b}}^{*}(f,g)\underline{\mathbf{a}}^{\mathrm{T}}(f,g)\right\}\end{aligned} \quad (44)$$

[4]To somewhat simplify the adopted notation, we assume that all the $(n^* - 1)$ interfering transmitters $\{T_{\mathrm{xf}}, f \neq g\}$ of Fig. 3 are in the payload phase. The generalization of the model (39) to the case where M out of $(n^* - 1)$ interfering transmitters radiate payload signals is direct and only requires minor formal modifications of (39).

[5]Without loss of generality, we may assume the parameter $\chi(f,g)$, $1 \leq f, g \leq n^*$, spanning the interval [0, 1]. This means that $\chi(f,g) = 1$ gives rise to the worst case when the MAI effects induced by T_{xf} on R_{xg} are maximum, while $\chi(f,g) = 0$ describes the lucky operating condition where no MAI is induced by T_{xf} on R_{xg}, $f \neq g$.

[6]Several measures support the conclusion that ν values of the order of 1/2 generally suffice to meet the aforementioned uncorrelation assumption among the rays impinging the receive antennas, at least in application scenarios as those considered here, where the terminals are (approximately) colocated at the same level over the ground [2], [10], [16], [17].

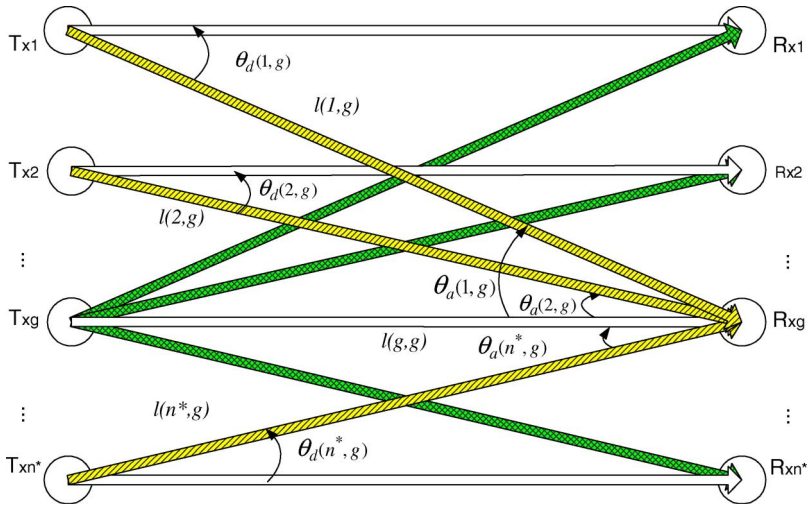

Fig. 3. Geometric model for the multiaccess spatial interference [16].

where $P^{(f)}$ is the power radiated by $T_{\rm xf}$, $\mathcal{N}_0$ in watts per Hertz is the thermal noise at $R_{\rm xg}$, and $\mathbf{R}_{\boldsymbol{\phi}}^{(f)} \triangleq E\{\underline{\boldsymbol{\phi}}^{(f)}(n)(\underline{\boldsymbol{\phi}}^{(f)}(n))^{\dagger}\}$ is the spatial covariance matrix of the signals generated by $T_{\rm xf}$.

VI. Some Game-Theory Concepts

In order to model the dynamic behavior of the "*ad hoc*" network of Fig. 3 composed by multiple mutually interfering pairs of transmit/receive nodes, we resort to the formal tool of the game theory [5] already employed to solve communication problems (see, for example, [19] and reference therein). We recall that a noncooperative and strategic game $G \triangleq \langle \mathbb{N}, \mathbb{A}, \{u_g\} \rangle$ has three components [5], [13]: a finite set $\mathbb{N} \triangleq \{1, 2, \ldots, n^*\}$ of players, a set A_g, $g \in \mathbb{N}$ of possible actions for each player, and a set of utility functions. Specifically, after denoting by $\mathbb{A} \triangleq A_1 \times A_2 \times \ldots \times A_{n^*}$ the space of action profiles [13], let us indicate as $u_g : \mathbb{A} \rightarrow \mathbb{R}$ the gth player's utility function. Thus, after indicating by $\underline{\mathbf{a}} \in \mathbb{A}$ an action profile, by $a_g \in A_g$ the players g's action in $\underline{\mathbf{a}}$, and by $\underline{\mathbf{a}}_{-g}$ the actions in $\underline{\mathbf{a}}$ of the other $(n^* - 1)$ players, we can say that $u_g(\underline{\mathbf{a}}) \equiv u_g(a_g, \underline{\mathbf{a}}_{-g})$ maps[7] each action profile $\underline{\mathbf{a}}$ into a real number [13]. In particular, in a strategic noncooperative game, each player chooses a suitable action $a_g^{\bullet}$ from his action set A_g to maximize its utility function, which is according to the following game rule [13]:

$$a_g^{\bullet} \equiv \max_{a_g \in A_g} u_g(a_g, \underline{\mathbf{a}}_{-g}). \tag{45}$$

Therefore, since there is no cooperation among the players, it is important to ensure the dynamic stability of the overall game. A concept related to this issue is the so-called NE. Simply stated, an NE is an action profile $\underline{\mathbf{a}}^{\star}$, at which no player may gain by unilaterally deviating [5], [13]. Therefore, NE is a stable operating point of the game because no player benefits from changing his strategy [4], [5]. More formally, an NE is an action profile $\underline{\mathbf{a}}^{\star}$, such that for all $a_g \in A_g$, the following inequality is satisfied [5], [13]:

$$u_g(a_g^{\star}, \underline{\mathbf{a}}_{-g}^{\star}) \geq u_g(a_g, \underline{\mathbf{a}}_{-g}^{\star}), \quad \forall g \in \mathbb{N}, \forall a_g \in A_g. \tag{46}$$

[7]The notation $u_g(a_g, \underline{\mathbf{a}}_{-g})$ emphasizes that the gth player controls only his own action a_g, but his achieved utility depends also on actions $\underline{\mathbf{a}}_{-g}$ taken by all other players [5], [13].

VII. Spatial Power-Allocation Multiantenna (SPAM) Game for *ad hoc* Networks

Let us focus now on the "*ad hoc*" network of Fig. 3 that is composed by n^* mutually interfering transmit/receive multiantenna units. The ultimate task of the gth transmit/receive pair is to maximize the information throughput $\mathbb{T}_{\rm G}(g), g = 1, \ldots, n^*$, which is sustained by the corresponding link $T_{\rm xg} \rightarrow R_{\rm xg}$ via suitable power allocation and shaping of the signals radiated by $T_{\rm xg}$. Since the signals radiated by the gth transmitter induces MAI over all other receivers $\{R_{xi}, i \neq g\}$ and the "*ad hoc*" nature of the network does not allow transmitters to exchange information (e.g., the transmitters do not cooperate), we may model the interaction between transmit/receive pairs as active, other than the network, as a noncooperative strategic game [1], [4], [5]. Specifically, in the considered "*ad hoc*" networking scenario of Fig. 3, the players' set $\mathbb{N}$ is composed of the n^* pairs of transmitters/receivers, while the set of actions A_g available to the gth player is the set of all the covariance matrices $\{\mathbf{R}_{\boldsymbol{\phi}}^{(g)}\}$ meeting the power constraint (16) so that we can pose

$$A_g \equiv \left\{ \mathbf{R}_{\boldsymbol{\phi}}^{(g)} : 0 \leq \text{Tra}\left[\mathbf{R}_{\boldsymbol{\phi}}^{(g)}\right] \leq t_g P_g \right\}, \quad g = 1, \ldots, n^*. \tag{47}$$

This means that the generic action a_g of $T_{\rm xg}$ consists of the transmission of a Gaussian distributed payload sequence with covariance matrix $\mathbf{R}_{\boldsymbol{\phi}}^{(g)}$. Furthermore, the utility function $u_g(.)$ for the gth transmit/receive pair is the conditional

throughput conveyed by the gth link so that we can write [see (23)]

$$\begin{aligned} u_g(\underline{\mathbf{a}}) &\triangleq u_g\left(\mathbf{R}_{\boldsymbol{\phi}}^{(1)},\ldots,\mathbf{R}_{\boldsymbol{\phi}}^{(g)},\ldots,\mathbf{R}_{\boldsymbol{\phi}}^{(n^*)}\right) \\ &\equiv \frac{1}{T_{\text{pay}}} I\left(\underline{\mathbf{y}}^{(g)};\underline{\vec{\phi}}^{(g)}|\hat{\mathbf{H}}_g\right) \\ &\equiv \lg\det\left(\mathbf{I}_{r_g}+\frac{1}{t_f}\left(\mathbf{K}_{\text{d}}^{(g)}\right)^{-1/2}\hat{\mathbf{H}}_g^{\text{T}}\mathbf{R}_{\boldsymbol{\phi}}^{(g)}\hat{\mathbf{H}}_g^{*}\right. \\ &\qquad \left.\times\left(\mathbf{K}_{\text{d}}^{(g)}\right)^{-1/2}+\sigma_{\varepsilon}^2(g)P^{(g)}\left(\mathbf{K}_{\text{d}}^{(g)}\right)^{-1}\right) \\ &\quad -\frac{1}{T_{\text{pay}}}\lg\det\left(\mathbf{I}_{r_g t_g}+\frac{\sigma_{\varepsilon}^2(g)T_{\text{pay}}}{t_g}\right. \\ &\qquad \left.\times\left(\left(\mathbf{K}_{\text{d}}^{(g)}\right)^{-1}\right)^{*}\otimes\mathbf{R}_{\boldsymbol{\phi}}^{(g)}\right) \end{aligned} \quad (48)$$

with the gth MAI covariance matrix $\mathbf{K}_{\text{d}}^{(g)}$ dependent on the spatial covariance matrices $\{\mathbf{R}_{\boldsymbol{\phi}}^{(i)}, i\neq g\}$ of the signals radiated by the interfering transmitters, as detailed by (44). About the rule of the game, each player (e.g., transmitter) chooses the action $\mathbf{R}_{\boldsymbol{\phi}}^{(g)\bullet}$ maximizing the throughput (48) conveyed by its own link; so, we can write [see (45)]

$$\mathbf{R}_{\boldsymbol{\phi}}^{(g)\bullet}\equiv\arg\max_{\mathbf{R}_{\boldsymbol{\phi}}^{(g)}\in A_g}\left\{\frac{1}{T_{\text{pay}}}I\left(\underline{\mathbf{y}}^{(g)};\underline{\vec{\phi}}^{(g)}|\hat{\mathbf{H}}_g\right)\right\} \qquad g=1,\ldots n^*. \quad (49)$$

A. Competitively Optimal Power-Allocation and Signal-Shaping Algorithms Under the Best-Effort and "Contracted QoS" Policies

In this section, we present the algorithms for the optimized power allocation and signal shaping for the network of Fig. 3 under "contracted QoS" and best-effort policies. Before proceeding, some remarks about the considered QoS policies are in order. We consider the QoS from an information-throughput point of view. Specifically, in "*ad hoc*" networks with no centralized controllers, it is not possible to ensure to any user a "guaranteed QoS." Thus, in place of guaranteed user's QoS, it is more reasonable, indeed, to resort to the concept of "contracted QoS" defined according to predefined multiple QoS classes. Therefore, the algorithm that we present attempts to achieve the target throughput classes desired by the users, and if these classes are not achievable due to the MAI, the algorithm attempts to achieve the next lower QoS classes by lowering the requested users' throughput. From this point of view, the best-effort strategy is a particular case of the "contracted QoS" one, where the number of QoS classes approaches infinity.

The algorithm for achieving the maximal throughput over the gth link under the above introduced "contracted QoS" policy is reported in Table I. It must be run by each transmit/receive pair that is active over the network of Fig. 3. In particular, the steps from 0 to 11 in Table I are setup procedures and eigen/singular values computations [these steps collect parameters' computation detailed from (27) to (32)], while $\text{TR}_{\text{TH}}^{(z)}$ (nats/slot) at the step 0 is the target throughput defining the zth QoS class. Step 12 verifies that the game is playable (e.g., the NE exists; see Section VI-B), while steps 13 and 14 set up the ρ parameter $\Im(\rho)$ and the step size Δ requested to carry out the power-allocation procedure (see also [11], [14], and [21]). The condition at step 15 assures that the power meets the constraint in (16), and the steps from 16 to 18 perform the competitively optimal power allocation and spatial signal shaping for the link $T_{\text{xg}}\rightarrow R_{\text{xg}}$. In steps 18 to 22, the convergence of the algorithm is checked by evaluating the difference between allocation at actual and previous iteration, and in step 23, the maximized information throughput sustained by gth link is evaluated. Finally, step 24 checks if the achieved throughput is compliant with the users' QoS requirements. If it is compliant, then the game stops. Otherwise, T_{xg} reduces the overall radiated power and restarts the game. If the obtained throughput is below the

TABLE I
PSEUDOCODE FOR THE IMPLEMENTATION OF THE POWER-ALLOCATION AND SIGNAL-SHAPING ALGORITHMS FOR THE gth TRANSMITTER/RECEIVER PAIR UNDER THE "CONTRACTED QoS" POLICY

0. Set the target throughput $TR_{TH}^{(z)}$ of the z-th QoS Classes ;
1. Initialize $\mathbf{R}_{\boldsymbol{\phi}}^{(g)}(new):=\mathbf{R}_{\boldsymbol{\phi}}^{(g)}(old)=[\mathbf{0}_{t_g\times t_g}]$;
2. fl(g)=1;
3. $\mathbb{T}_G(g)=0$;
4. $\alpha^{(g)}\triangleq(\tilde{P}T_{tr}/r_g)Tra[(\mathbf{K}_d^{(g)})^{-1}]$;
5. $\sigma_{\varepsilon}^2(g)\triangleq(1+\alpha^{(g)}/t_g)^{-1}$;
6. Compute and sort the r eigenvalues of $\mathbf{K}_d^{(g)}$;
7. Compute the SVD of $\hat{\mathbf{H}}_g^{*}\mathbf{K}_d^{(g)-1}\hat{\mathbf{H}}_g^{T}$;
8. Sort the $s\triangleq min(r,t)$ eigenvalues $\{k_1^{(g)2},...,k_s^{(g)2}\}$ of $\mathbf{K}_d^{(g)}$;
9. $\alpha_m^{(g)}\triangleq\mu_m^{(g)}k_m^{(g)2}/t_g(\mu_m^{(g)}+P^{(g)}\sigma_{\varepsilon}^2(g))$;
10. $\beta_l^{(g)}\triangleq\sigma_{\varepsilon}^2(g)T_{pay}/\mu_l^{(g)}t_g$;
11. $\mu_{min}^{(g)}\triangleq\min_{1\leq l\leq r}\{\mu_m^{(g)}\}$, $\beta_{max}^{(g)}\triangleq\frac{\sigma_{\varepsilon}^2(g)T_{pay}}{\mu_{min}^{(g)}t_g}$;
12. if $k_m^{(g)2}\geq(\mu_m^{(g)}+P^{(g)}\sigma_{\varepsilon}^2(g))\frac{\sigma_{\varepsilon}^2(g)\sqrt{rT_{pay}}}{\mu_{min}^{(g)}\mu_m^{(g)}}$ for all m and fl(g)=1
{
13. Set $\rho^{(g)}:=0$ and $\Im(\rho^{(g)}):=\emptyset$;
14. Set the step size Δ;
15. While $\left(\sum_{m\in\Im(\rho^{(g)})}P^{\star(g)}(m)<Pt_g\right)$ do
{
16. Update $\rho^{(g)}=\rho^{(g)}+\Delta$;
17. Update the set $\Im(\rho^{(g)})$ via eq. (36);
18. Compute the powers and the covariance matrix via eq.(33), (34), (37);
19. Set $\Psi^{(g)}:=\mathbf{R}_{\boldsymbol{\phi}}^{(g)}(new)-\mathbf{R}_{\boldsymbol{\phi}}^{(g)}(old)$;
20. If $(||\Psi||_E^2\leq 0.05||\mathbf{R}_{\boldsymbol{\phi}^{(g)}}^{(g)}(old)||_E^2)$
21. then fl(g)=0, else fl(g)=1;
22. $\mathbf{R}_{\boldsymbol{\phi}}^{(g)}(old):=\mathbf{R}_{\boldsymbol{\phi}}^{(g)}(new)$
}
23. Evaluate $\mathbb{T}_G(g)$ via (38) for the g-th link;
24. if $\mathbb{T}_G(g)=TR_{TH}^{(z)}$ stop; else
25. if $\mathbb{T}_G(g)>TR_{TH}^{(z)}$ reduce the radiated power $P^{(g)}$ and go to Step 1, else
26. if $\mathbb{T}_G(g)<TR_{TH}^{(z)}$ lower the target class to z-1 and go to Step 1;
}

TABLE II
PSEUDOCODE FOR THE ASYNCHRONOUS AND DISTRIBUTED IMPLEMENTATION OF THE SPAM GAME

```
For all k such that τ_k ∈ ϒ
{ For all terminals g ∈ ℕ such that τ_k ∈ ϒ_g
    { Evaluate the MAI matrix K_d^(g) ;
      Run the algorithm of Table I so to compute φ⃗^(g)• and R_φ^(g)•;
      Radiate the signal vector φ⃗^(g)•;
    }
}
```

requested $\mathrm{TR}_{\mathrm{TH}}^{(z)}$, the transmitter T_{xg} restarts the game with a target throughput $\mathrm{TR}_{\mathrm{TH}}^{(z-1)}$ that is lower than the original $\mathrm{TR}_{\mathrm{TH}}^{(z)}$.

B. Distributed and Asynchronous Implementation of the SPAM Game

Let us assume that the algorithm reported in Table I is iteratively run (possibly, in an asynchronous way) by all transmit/receive pairs active over the network of Fig. 3. Specifically, after measuring the impairing MAI covariance matrix $\mathbf{K}_{\mathrm{d}}^{(1)}$, the first $T_{\mathrm{x1}} \rightarrow R_{\mathrm{x1}}$ pair begins to update its power allocation and signal shaping by running the algorithm of Table I. Thus, this algorithm is successively run by the second pair $T_{\mathrm{x2}} \rightarrow R_{\mathrm{x2}}$, the third one, etc. Hence, the algorithm is applied again by the first pair, the second one and so on.[8] Formally, as in [1], in the fully asynchronous and distributed implementation of the SPAM game, the gth transmit/receive pair of Fig. 3 executes the power-control and signal-shaping algorithms of Table I at time instances given by the set $\Upsilon_g \stackrel{\Delta}{=} \{t_{g_1}, t_{g_2}, t_{g_3} \ldots\}$ with $t_{g_i} < t_{g_{(i+1)}}$. Thus, after indicating by $\Upsilon \stackrel{\Delta}{=} \{\tau_1, \tau_2, \tau_3, \ldots\}$ the overall set of update instants $\Upsilon_1 \bigcup \Upsilon_2 \ldots \bigcup \Upsilon_{n^*}$ sorted in the increased order, the asynchronous and distributed implementation of the considered SPAM game generates the sequence of power allocations and signal shapings following the iterative procedure detailed in Table II. At this stage, it is important to note, as anticipated in Section I, that the proposed algorithm is not centralized and fully scalable, because the computational cost does not depend on the number of users in the network.

Thus, about the asynchronous and distributed implementation of the SPAM game reported in Table II, the key questions are the following.

1) Does NE exist for the SPAM game?
2) Is the NE unique?
3) Does the above iterative algorithm converge toward the NE?

The following Proposition 3 presents sufficient conditions for the existence, uniqueness, and achievability of the NE. From a formal point of view, Proposition 3 represents the main analytical result of this contribution.

Proposition 3: With reference to the asynchronous and distributed implementation of the SPAM game reported by Table II, let us assume that the following three conditions are met:

$$k_m^{(g)2} > \left(1 + \frac{\sigma_\varepsilon^2(g) P^{(g)}}{\mu_m^{(g)}}\right)\left(\frac{t}{\rho^{(g)}} + \sigma_\varepsilon^2(g)\mathrm{Tra}\left[\left(\mathbf{K}_{\mathrm{d}}^{(g)}\right)^{-1}\right]\right)$$

$$1 \leq m \leq \min\{r_g, t_g\}, \quad 1 \leq g \leq n^* \tag{50}$$

$$r_g \geq t_g, \quad 1 \leq g \leq n^* \tag{51}$$

$$T_{\mathrm{pay}} \gg t_g > 1 \text{ and/or } \sigma_\varepsilon^2(g) \rightarrow 0, \quad 1 \leq g \leq n^*. \tag{52}$$

Thus, the NE of the SPAM game exists, and it is unique. Furthermore, the distributed and asynchronous implementation of the SPAM game of Table II converges to the NE from any starting point.

A sketch of the proof of Proposition 3 is reported in the final Appendices.

VIII. NUMERICAL RESULTS AND CONCLUSION

To test the effectiveness of the proposed SPAM algorithm, several numerical tests have been carried out. The obtained results about the achieved throughput are detailed in the following sections.

A. Achieved Network Throughput

Fig. 4 depicts the squared network considered for the tests. It is composed by two transmit/receive pairs equipped with $t = 4$ and $r = 8$ transmit/receive antennas and operating at $\mathrm{SNR} = 10$ dB with $T_{\mathrm{pay}} = 120$. The numerical tests have been carried out under the best-effort policy. At the beginning (e.g., at zeroth iteration), only the first transmit/receive pair is ON (see Fig. 4). By running the SPAM game, we obtain an information throughput around 18 bits/slots for the first pair (see Fig. 5), while the throughput sustained by the second link $T_{\mathrm{x2}} \rightarrow R_{\mathrm{x2}}$ is (obviously) zero. Next, the link $T_{\mathrm{x2}} \rightarrow R_{\mathrm{x2}}$ is activated; so, the throughput on the $T_{\mathrm{x1}} \rightarrow R_{\mathrm{x1}}$ link decreases to 13 bits/slot (see Fig. 5), while the throughput of the $T_{\mathrm{x2}} \rightarrow R_{\mathrm{x2}}$ link increases until the same value. In this case, we have considered the absence of obstacles between interferers (e.g., $\chi^2(1,2) = \chi^2(2,1) = 1$). This point represents the (first) NE for the considered squared topology, and it has reached and achieved 23 iterations (see Fig. 5). Next, the network topology changes, and an obstacle is introduced between the second transmitter and first receiver, so that $\chi^2(1,2) = 0.6$, while $\chi^2(2,1) = 1$. As it is shown in Fig. 5, the new NE (achieved at the 60th iteration) is characterized by different values of the achieved throughput over the active links. After this, we considered an operating scenario with $\chi^2(1,2) = 0.8$ and $\chi^2(2,1) = 1$. In this case, the SPAM game gives rise to an information throughput over the link $T_{\mathrm{x1}} \rightarrow R_{\mathrm{x1}}$ limited up to 14.3 bits/slot (see Fig. 5). After this, we introduce an additional change in the network topology, so that both receivers do not suffer from MAI (e.g., $\chi^2(1,2) = \chi^2(2,1) = 0$; see Fig. 4). In this operating condition, the sustained link throughput increases to approach a new NE, where the throughput conveyed by both links equates 19.2 bits/slot (see Fig. 5). Finally, we assumed

[8] In an asynchronous implementation of the game, the updating ordering may also change from time to time, possibly in a random way [13].

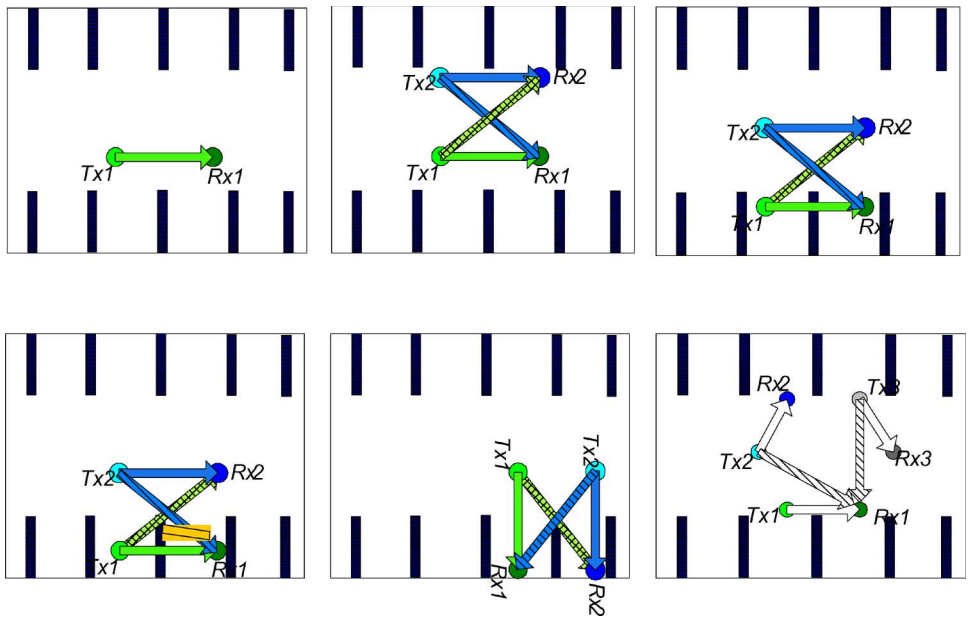

Fig. 4. Network topology sequence considered in Section VIII for the numerical tests. $T_{\mathrm{xg}} \rightarrow R_{\mathrm{xg}}$, $g = 1, 2, 3$ are the desired links, while $T_{\mathrm{xg}} \rightarrow R_{\mathrm{xf}}$, $g \neq f$ are the interfering ones.

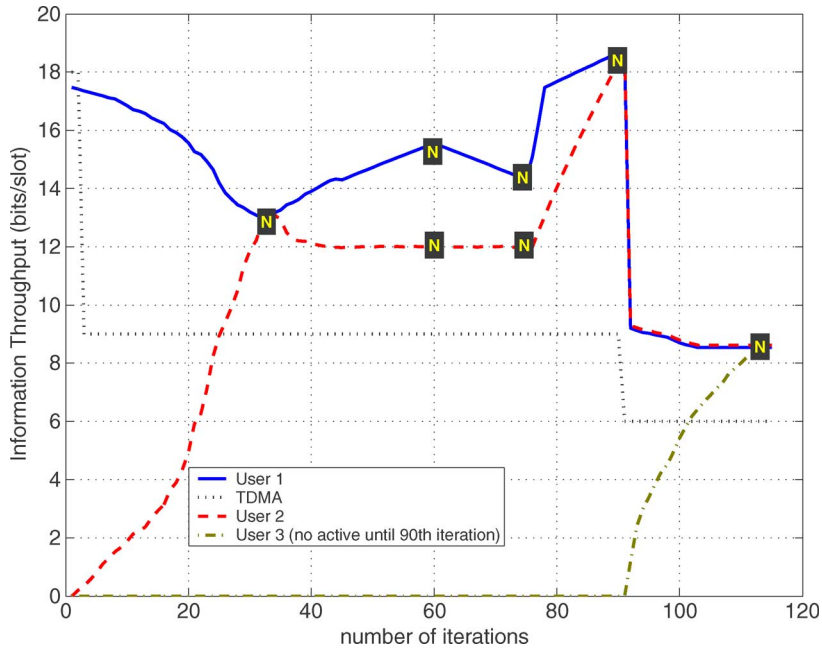

Fig. 5. Information throughput achieved by the SPAM game and TDMA under the best-effort policy for the network topology sequence of Fig. 4.

that a third pair of transmit/receive units switches ON, so that the network assumes the hexagonal topology of Fig. 4. The new NE achieved by running the SPAM game approaches 8.3 bits/slot for all active links (see Fig. 5).

B. Effects of Mismatches in the Evaluation of the MAI Covariance Matrix

The accuracy in the estimate $\overset{\vee}{\mathbf{K}}_{\mathrm{d}}$ in (5) of the actual MAI covariance matrix $\mathbf{K}_{\mathrm{d}}$ is mainly limited by the length T_{L} of the employed learning phase. To test the sensitivity of the proposed power-allocation algorithm of Table I on errors possibly affecting the estimated matrix $\overset{\vee}{\mathbf{K}}_{\mathrm{d}}$, we have perturbed the actual $\mathbf{K}_{\mathrm{d}}$ via a randomly generated $(r \times r)$ matrix $\mathbf{N}$, which is composed by zero-mean proper complex unit-variance independent Gaussian elements. This was accomplished according to the following relationship:

$$\overset{\vee}{\mathbf{K}}_{\mathrm{d}} = \mathbf{K}_{\mathrm{d}} + \sqrt{\frac{\|\mathbf{K}_{\mathrm{d}}\|_E^2}{r^2}}\sqrt{\delta}\mathbf{N}$$

where $\delta \triangleq E\{\|\mathbf{K}_{\mathrm{d}} - \overset{\vee}{\mathbf{K}}_{\mathrm{d}}\|_E^2 / \|\mathbf{K}_{\mathrm{d}}\|_E^2$ is a deterministic parameter set according to the desired squared estimation errors affecting $\overset{\vee}{\mathbf{K}}_{\mathrm{d}}$. Thus, using this perturbed covariance matrix $\overset{\vee}{\mathbf{K}}_{\mathrm{d}}$ (with $\delta = 0.05$) in place of the actual one $\mathbf{K}_{\mathrm{d}}$, we have

TABLE III
NASH-EQUILIBRIA COMPARISON FOR PERFECTLY KNOWN MAI COVARIANCE MATRIX AND IMPERFECTLY KNOWN MAI COVARIANCE MATRIX ($\delta = 0.05$)

Nash Equilibrium (bits/slot)	Nash Equilibrium (perturbed $\mathbf{K}_d$) (bits/slot)	percentage loss
(13,13,0)	(12.5,12.5,0)	3.98%
(15.6,12.1,0)	(15.2, 11.8,0)	2.5%
(14.3,12,0)	(13.8,11.4,0)	4.1%
(19.2,19.2,0)	(18.9, 18.9,0)	1.5%
(8.3,8.3,8.3)	(8.15, 8.15, 8.15)	1.8%

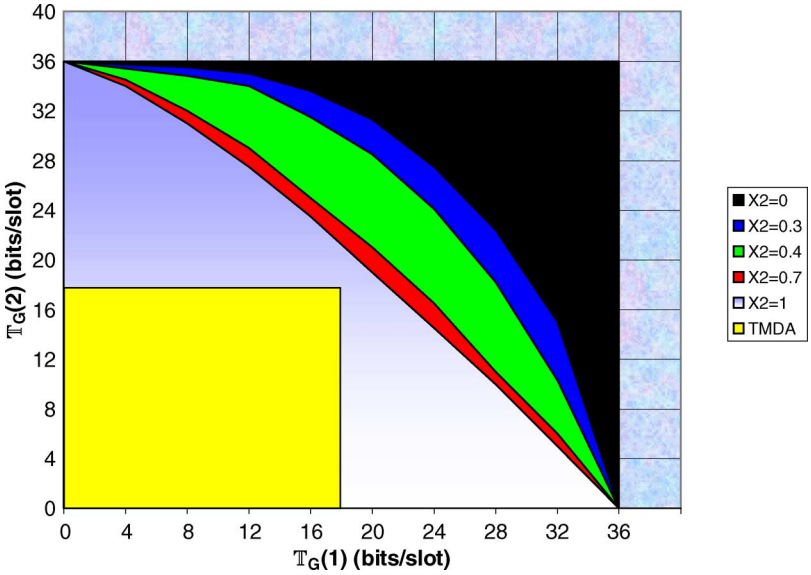

Fig. 6. Regions for the information throughput achieved by the proposed SPAM game and TDMA for a squared network topology and different values of the shadowing factors $\chi^2(1,2) \equiv \chi^2(2,1) \equiv \chi^2$.

performed the power allocation as indicated by the relationships (33) and (34). Then, we have evaluated the resulting conditional throughput $\mathbb{T}_G(\hat{\mathbf{H}})$ via (38), for the scenario depicted in Fig. 4. The values in Table III report the values of NE when we consider perfect MAI covariance matrix knowledge and MAI covariance matrix affected by estimation errors. The last column of Table III points out that the resulting throughput loss is limited up to 4% for the considered value of the δ parameter. In the first row, it is possible to appreciate that the performance loss is within 4%, because the value of the throughput is 12.5 in place of 13.

C. Achievable Throughput Regions

In Fig. 6, we report the achievable throughput regions of a squared network composed by two transmit/receive pairs for different values of the shadowing factors $\chi^2(1,2) = \chi^2(2,1)$. These regions represent the pairs of information throughput (R_1, R_2), in which the links that are active over the considered network may guarantee when the proposed SPAM game is run. After comparing the throughput regions guaranteed by the proposed SPAM game with those of conventional TDMA orthogonal access method (see the inner square in Fig. 6), we may conclude that at $\chi^2(1,2) = \chi^2(2,1) < 0.7$ (e.g., in the presence of strong MAI), the proposed SPAM game outperforms the conventional TDMA one. In Fig. 7, the throughput region for the hexagonal network topology, with all χ equating 0.5, is shown. Fig. 6 points out that the throughput achievable by the SPAM game outperforms that of TDMA.

D. Spam Game Versus TDMA: A Throughput Comparison

The above conclusion is also supported by the dotted curve of Fig. 5, which reports the throughput achieved by the TDMA strategy for the same networking scenarios previously considered in Section VIII-A. In fact, an examination[9] of Fig. 5 shows that although the TDMA is a centralized technique assuring orthogonal (e.g., collision free) multiple access, nevertheless, the corresponding throughput is below those achieved by running the proposed SPAM game, especially when the MAI effects are substantial. Overall, the SPAM game-versus-TDMA comparison of Figs. 5 and 6 supports the superiority of decentralized competitively optimal access strategies over centralized orthogonal ones, at least in networking scenarios where the spatial dimension of the system may be efficiently exploited to perform the MAI suppression. As anticipated in Section I, this can be justified [21] by observing that, although (perfectly synchronous) TDMA does not present interference

[9]Under the above stated assumptions about the considered network in Fig. 4, the same throughput values marked by the dotted plot of Fig. 5 are also achieved when alternative orthogonal centralized access strategies (as, for example, CDMA or FDMA) are implemented.

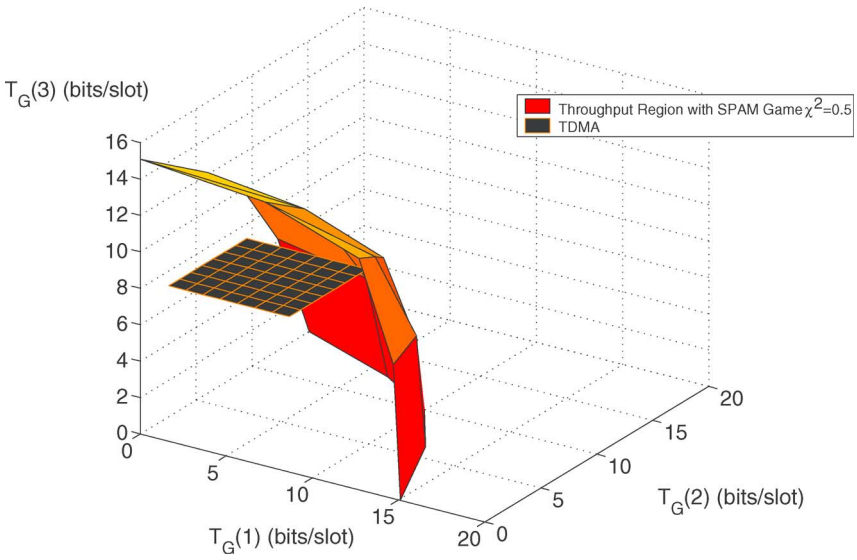

Fig. 7. Regions for the information throughput achieved by the proposed SPAM Game and TDMA for a hexagonal network topology and all shadowing factors equal to $\chi^2 = 0.5$.

for the receiver, it assigns a slot out of $n^\star$; so, the capacity is reduced with respect to a single-user case. On the contrary, in the proposed approach, there is the presence of interference, but through a signal shaping, its effect is reduced while the capacity has not to be divided by $n^\star$ because it is based on continuous transmission. An additional feature is that the TDMA outperforms the proposed approach for a very low number of antennas (one or two), because signal shaping is not able to counterbalance the effect of interference (see [21]).

This conclusion may be of actual interest for a "plug-and-play" planning of multiantenna "*ad hoc*" networking architectures. From this point of view, the results presented in this paper probably grasp only the tip of the iceberg.

Appendix I
Existence of an NE for the SPAM Game

To prove the existence of the NE for the distributed and asynchronous implementation of the SPAM game reported in Table II, we resort to the following general result from [1] and [13] about noncooperative strategic games.

Proposition 4—Existence of an NE: An NE exists in a noncooperative strategic game $G \triangleq \langle \mathbb{N}, \mathbb{A}, \{u_g\} \rangle$ if, for all $g = 1, \ldots, n^*$.

1) The set A_g is not empty, compact, and convex. (53)
2) The utility function $u_g(\underline{\mathbf{a}})$ is continuous over $\underline{\mathbf{a}} \in \mathbb{A}$. (54)
3) The utility function $u_g(a_g, \underline{\mathbf{a}}_{-g})$ is quasi-concave[10] in $a_g \in A_g$ for any assigned $\underline{\mathbf{a}}_{-g}$. (55)

Thus, our next task is to prove that the SPAM game of Table II meets all of the above conditions.

[10]See [15] for the definition and properties of the quasi-concave functions. We only stress that a concave function is also quasi-concave [15].

Condition (53): For all values of g, the set of actions A_g in (47) is limited between the null matrix and the matrix $\mathbf{R}_{\boldsymbol{\phi}}^{(g)}(\max)$ with $\mathrm{Tra}[\mathbf{R}_{\boldsymbol{\phi}}^{(g)}(\max)] \equiv t_g P_g$. This set is closed because the boundary of the set [e.g., the null matrix and the maximum matrix $\mathbf{R}_{\boldsymbol{\phi}}^{(g)}(\max)$] falls into the set A_g. Therefore, because the set is closed and bounded, it is also compact. In addition, this set is also convex. In fact, after considering two generic elements $\mathbf{R}_{\boldsymbol{\phi}}^{(g)}(1)$ and $\mathbf{R}_{\boldsymbol{\phi}}^{(g)}(2)$ of the set A_g, we have that the combined matrix

$$\overline{\mathbf{R}}_{\boldsymbol{\phi}}^{(g)} \triangleq \lambda \mathbf{R}_{\boldsymbol{\phi}}^{(g)}(1) + (1-\lambda)\mathbf{R}_{\boldsymbol{\phi}}^{(g)}(2), \qquad 0 \le \lambda \le 1 \quad (56)$$

is also in A_g, because its trace

$$\mathrm{Tra}\left[\overline{\mathbf{R}}_{\boldsymbol{\phi}}^{(g)}\right] = \lambda \mathrm{Tra}\left[\mathbf{R}_{\boldsymbol{\phi}}^{(g)}(1)\right] + (1-\lambda)\mathrm{Tra}\left[\mathbf{R}_{\boldsymbol{\phi}}^{(g)}(2)\right] \quad (57)$$

falls in the interval $[0, t_g P_g]$. Thus, the set A_g is convex.

Condition (54): Since the function $\lg\det[\mathbf{M}]$ is continuous in the elements of the matrix $\mathbf{M}$, in order to prove the continuity of the utility function $u_g(.)$ in (48) in the (matrix) arguments $\{\mathbf{R}_{\boldsymbol{\phi}}^{(1)} \ldots \mathbf{R}_{\boldsymbol{\phi}}^{(n^*)}\}$, it suffices to test the continuity of the two terms enclosed by the squared brackets in (48). Since both of these terms are continuous in the gth argument $\mathbf{R}_{\boldsymbol{\phi}}^{(g)}$, and in addition, $\mathbf{K}_{\mathrm{d}}^{-1}$ is also continuous in $\{\mathbf{R}_{\boldsymbol{\phi}}^{(i)}, i \ne g\}$ because $\mathbf{K}_{\mathrm{d}}$ in (44) is the linear superposition of $\{\mathbf{R}_{\boldsymbol{\phi}}^{(i)}, i \ne g\}$, we conclude that $u_g(.)$ in (48) meets the continuity property (54).

Condition (55): After recalling that a concave function is also quasi-concave [15], it suffices to prove that the utility function $u_g(.)$ in (48) is concave in $\mathbf{R}_{\boldsymbol{\phi}}^{(g)}$ for any assigned $\mathbf{K}_{\mathrm{d}}^{(g)}$. To accomplish this task, we simply observe that the $\lg\det[\mathbf{M}]$ function is concave in $\mathbf{M}$, so that $u_g(.)$ in (48) is concave in $\mathbf{R}_{\boldsymbol{\phi}}^{(g)}$ when the term following the minus sign in (48) becomes negligible. An examination of (48) leads to the conclusion that this term becomes negligible when the available channel

estimates $\hat{\mathbf{H}}$ are very reliable (e.g., $\sigma_{\varepsilon}^2(g)$ in (48) vanishes), when $T_{\rm pay}$ is large, or when all the inequalities in (50) are met. These last considerations complete the proof about the existence of an NE for the SPAM game of Table II.

APPENDIX II
UNIQUENESS AND ACHIEVABILITY OF THE NE FOR THE SPAM GAME

To prove the uniqueness of NE for the SPAM game of Table II, we resort to some basic results reported in [1] and [4] about the so-called standard functions. Formally, according to a current taxonomy [1], [4], for any assigned (n^*-1)-ple of spatial covariance matrices $\{\mathbf{R}_{\boldsymbol{\phi}}^{(i)}, i \neq g\}$, the resulting maximizing $\mathbf{R}_{\boldsymbol{\phi}}^{(g)\bullet}$ in (49) constitutes the so-called "gth terminal best response" to the set $\{\mathbf{R}_{\boldsymbol{\phi}}^{(i)}, i \neq g\}$ of interfering covariance signal matrices. Therefore, for any assigned n^*-ple $\{\mathbf{R}_{\boldsymbol{\phi}}^{(i)}, i = 1, \ldots, n^*\}$, we may collect the resulting terminals best responses $\{\mathbf{R}_{\boldsymbol{\phi}}^{(g)\bullet}, g = 1, \ldots, n^*\}$ in (49) into the so-called matrix of best responses (MBR) $[\underline{\mathbf{B}}^{\bullet}]$, which is formally defined as (see [1] and [4])

$$[\underline{\mathbf{B}}^{\bullet}]\left(\mathbf{R}_{\boldsymbol{\phi}}^{(1)}, \ldots, \mathbf{R}_{\boldsymbol{\phi}}^{(n)}\right) \triangleq [\mathbf{R}_{\boldsymbol{\phi}}(1)^{\bullet}, \ldots, \mathbf{R}_{\boldsymbol{\phi}}(n^*)^{\bullet}]^{\rm T}. \quad (58)$$

According to [1] and [4], from an analytical point of view, the MBR $[\underline{\mathbf{B}}^{\bullet}](.)$ in (58) constitutes a standard function when it meets the following three properties:

Positiveness:

$$1)\ \forall \underline{\mathbf{a}} \triangleq \left(\mathbf{R}_{\boldsymbol{\phi}}^{(1)}, \ldots, \mathbf{R}_{\boldsymbol{\phi}}^{(n^*)}\right) \in \mathbb{A} \quad \text{then } [\underline{\mathbf{B}}^{\bullet}]\left(\mathbf{R}_{\boldsymbol{\phi}}^{(1)}, \ldots, \mathbf{R}_{\boldsymbol{\phi}}^{(n^*)}\right) \trianglerighteq \underline{\mathbf{0}} \quad (59)$$

Monotonicity:

$$2)\ \text{if } \mathbf{R}_{\boldsymbol{\phi}}^{(g)} \trianglerighteq \overline{\mathbf{R}_{\boldsymbol{\phi}}^{(g)}},\ \text{then } [\underline{\mathbf{B}}^{\bullet}]\left(\mathbf{R}_{\boldsymbol{\phi}}^{(1)}, \ldots, \mathbf{R}_{\boldsymbol{\phi}}^{(n^*)}\right) \trianglerighteq [\underline{\mathbf{B}}^{\bullet}]\left(\overline{\mathbf{R}_{\boldsymbol{\phi}}^{(1)}}, \ldots, \overline{\mathbf{R}_{\boldsymbol{\phi}}^{(n^*)}}\right) \quad (60)$$

Scalability:

$$3)\ \forall\, c \geq 1,\ \text{then } c[\underline{\mathbf{B}}^{\bullet}]\left(\mathbf{R}_{\boldsymbol{\phi}}^{(1)}, \ldots, \mathbf{R}_{\boldsymbol{\phi}}^{(n^*)}\right) \trianglerighteq [\underline{\mathbf{B}}^{\bullet}]\left(c\mathbf{R}_{\boldsymbol{\phi}}^{(1)}, \ldots, c\mathbf{R}_{\boldsymbol{\phi}}^{(n^*)}\right) \quad (61)$$

where the expression $\mathbf{Q} \triangleright \mathbf{U} (\mathbf{Q} \trianglerighteq \mathbf{U})$ means that $\mathbf{Q}-\mathbf{U}$ is a definite (semidefinite) positive matrix. Therefore, since [4, Th. 1] assures the uniqueness of the NE when the corresponding MBR is a standard function (see also [1] for additional details on this topic), our next task is to prove that the MBR $[\underline{\mathbf{B}}^{\bullet}](.)$ in (58) of the considered SPAM game meets all the properties (59)–(61).

1) Positiveness—In order to prove the positiveness of $[\underline{\mathbf{B}}^{\bullet}](.)$ for the SPAM game of Table II, it suffices to test that all the best response matrices $\{\mathbf{R}_{\boldsymbol{\phi}}^{(g)\bullet}, g = 1, \ldots, n^*\}$ in (58) are definite positive for any assigned MAI matrices $\{\mathbf{K}_{\rm d}^{(g)}, g = 1, \ldots, n^*\}$. By examining the expression of $\mathbf{R}_{\boldsymbol{\phi}}^{(g)\bullet}$ reported in (37), we conclude that $\mathbf{R}_{\boldsymbol{\phi}}^{(g)\bullet}$ is positive when $t_g \leq s_g \triangleq \min\{r_g, t_g\}$ and all the powers $\{P_g^*(m)\}$ in (33) and (34) are strictly positive. In turn, both these conditions are met when the inequalities (50) and (51) are fulfilled.
2) Monotonicity—In order to prove the monotonicity property, we have to test the validity of the following inequalities:

$$u_g\left(\mathbf{R}_{\boldsymbol{\phi}}^{(g)}; \overline{\mathbf{K}}_{\rm d}^{(g)}\right) \leq u_g\left(\mathbf{R}_{\boldsymbol{\phi}}^{(g)}; \mathbf{K}_{d}^{(g)}\right), \quad \forall \overline{\mathbf{K}}_{\rm d}^{(g)} \trianglerighteq \mathbf{K}_{\rm d}^{(g)} \quad (62)$$

$$u_g\left(\mathbf{R}_{\boldsymbol{\phi}}^{(g)}; \mathbf{K}_{\rm d}^{(g)}\right) \leq u_g\left(\overline{\mathbf{R}}_{\boldsymbol{\phi}}^{(g)}; \mathbf{K}_{\rm d}^{(g)}\right), \quad \forall \overline{\mathbf{R}}_{\boldsymbol{\phi}}^{(g)} \trianglerighteq \mathbf{R}_{\boldsymbol{\phi}}^{(g)}. \quad (63)$$

For testing (62), we simply note that since the utility function in (48) is composed by the function $\log\det(\mathbf{I}+\mathbf{A})$, we have that this last can be rewritten as $\log(\sum(1+\lambda_a))$, where $\{\lambda_a\}$ are the eigenvalues of $\mathbf{A}$. Thus, $\log\det(\mathbf{I}+\mathbf{A})$ increases for increasing $\{\lambda_a\}$. Now, when $\overline{\mathbf{K}}_{\rm d}^{(g)} \trianglerighteq \mathbf{K}_{\rm d}^{(g)}$, we have that $\overline{k}_m^{(g)2} \geq k_m^{(g)2}, \forall m$. This implies that the eigenvalues of the matrix in (48) act as a reference to the matrix $\mathbf{K}_{\rm d}^{(g)-1}$, so we have that, when $\overline{\mathbf{K}}_{\rm d}^{(g)} \trianglerighteq \mathbf{K}_{\rm d}^{(g)}$, $u_g(.)$ decreases. By applying the same proof arguments to the matrix $\mathbf{R}_{\boldsymbol{\phi}}^{(g)}$, we directly arrive, at test, the monotonic increasing behavior of the function $u_g(.)$ in (48) with respect to $\mathbf{R}_{\boldsymbol{\phi}}^{(g)}$. This proves the validity of inequality (63).
3) Scalability—For any assigned (n^*-1)-ple $\{\mathbf{R}_{\boldsymbol{\phi}}^{(i)}, i = 1, \ldots, n^*; i \neq g\}$, let us indicate by $\mathbf{K}_{\rm d}^{(g)}$ the resulting MAI covariance matrix computed according to the model (44), and let us denote $\overline{\mathbf{K}}_{\rm d}^{(g)}$ as the corresponding MAI matrix generated by the (n^*-1)-ple $\{c\mathbf{R}_{\boldsymbol{\phi}}^{(i)}, i = 1, \ldots, n^*; i \neq g\}$. Therefore, by definition, the proof of the scalability property in (61) is equivalent to test the validity of the following inequality:

$$c \arg \max_{\mathbf{R}_{\boldsymbol{\phi}}^{(g)} \in A_g} \left\{u_g\left(\mathbf{R}_{\boldsymbol{\phi}}^{(g)}; \mathbf{K}_{\rm d}^{(g)}\right)\right\} \triangleright \arg \max_{\mathbf{R}_{\boldsymbol{\phi}}^{(g)} \in A_g} \left\{u_g\left(\mathbf{R}_{\boldsymbol{\phi}}^{(g)}; \overline{\mathbf{K}}_{\rm d}^{(g)}\right)\right\}, \quad g = 1, \ldots, n^*. \quad (64)$$

Now, we observe that when $\mathbf{K}_{\rm d}^{(g)}$ and $\overline{\mathbf{K}}_{\rm d}^{(g)}$ are computed according to the MAI model in (44), then they satisfy the following chain of inequalities:

$$c\mathbf{K}_{\rm d}^{(g)} \triangleright \overline{\mathbf{K}}_{\rm d}^{(g)} \triangleright \mathbf{K}_{\rm d}^{(g)}. \quad (65)$$

Therefore, since we have already proved that $u_g(.)$ in (48) increases for increasing $\mathbf{K}_{\mathrm{d}}^{(g)}$, the validity of (64) directly arises from the inequality chain (65). After proving the uniqueness of the NE for the SPAM game in Table II, its availability is directly guaranteed by the fact that the NE represents the unique stable operating point of the game [13].

REFERENCES

[1] C. Saraydar, N. B. Mandayanan, and D. J. Goodman, "Efficient power control via pricing in wireless data networks," *IEEE Trans. Commun.*, vol. 50, no. 2, pp. 291–303, Feb. 2002.

[2] C.-N. Chuan, N. D. S. Tse, J. M. Kahn, and R. A. Valenzuela, "Capacity-scaling in MIMO wireless systems under correlated fading," *IEEE Trans. Inf. Theory*, vol. 48, no. 3, pp. 637–650, Mar. 2002.

[3] E. Baccarelli and M. Biagi, "Error resistant space-time coding for emerging 4G-WLANs," in *Proc. WCNC*, Mar. 2003, pp. 72–77.

[4] R. Yates, "A framework for uplink power control in cellular radio systems," *IEEE J. Sel. Areas Commun.*, vol. 13, no. 7, pp. 1341–1347, Sep. 1995.

[5] A. B. MacKenzie and S. B. Wicker, "Game theory in communications: Motivation, explanation and application to power control," in *Proc. GLOBECOM*, 2001, pp. 821–825.

[6] P. Lancaster and M. Tismetesky, *The Theory of Matrices*, 2nd ed. New York: Academic, 1985.

[7] R. G. Gallagher, *Information Theory and Reliable Communication*. Hoboken, NJ: Wiley, 1968.

[8] S. Verdu and T. S. Han, "A general formula for channel capacity," *IEEE Trans. Inf. Theory*, vol. 40, no. 6, pp. 1147–1157, Jul. 1994.

[9] C. E. Perkins, *Ad Hoc Networking*. Reading, MA: Addison-Wesley, 2000.

[10] A. J. Paulraj, D. A. Gore, R. U. Nabar, and H. Bolcskei, "An overview of MIMO communications: A key to gigabit wireless," *Proc. Inst. Electr. Eng.*, vol. 92, no. 2, pp. 198–218, Feb. 2004.

[11] E. Baccarelli and M. Biagi, "Optimized power allocation and signal shaping for interference-limited multi-antenna '*ad hoc*' networks," in *Proc. PWC*, Sep. 2003, pp. 138–152.

[12] A. Lozano, A. M. Tulino, and S. Verdù, "Multiple-antenna capacity in the low-power regime," *IEEE Trans. Inf. Theory*, vol. 49, no. 10, pp. 2527–2544, Oct. 2003.

[13] M. J. Osborne and A. Rubinstein, *A Course in Game Theory*. Cambridge, MA: MIT Press, 1994.

[14] E. Baccarelli, M. Biagi, and C. Pelizzoni, "Optimized signal shaping for multi-antenna networks impaired by multiple access interference," INFO-COM Univ. Rome, Rome, Italy. Tech. Rep. [Online]. Available: http://infocom.uniroma1.it/~biagi/mimocol.pdf

[15] J. Ponstein, "Seven kinds of convexity," *SIAM Rev.*, vol. 9, no. 1, pp. 115–119, Jan. 1967.

[16] F. R. Farrokhi, G. J. Foschini, A. Lozano, and R. A. Valenzuela, "Link-optimal space-time processing with multiple transmit and receive antennas," *IEEE Commun. Lett.*, vol. 5, no. 3, pp. 85–87, Mar. 2001.

[17] A. Paulraj, R. Nabar, and D. Gore, *Introduction to Space-Time Wireless Communications*. Cambridge, U.K.: Cambridge Univ. Press, 2003.

[18] C. Rose, S. Ulukus, and R. D. Yates, "Wireless systems and interference avoidance," *IEEE Trans. Wireless Commun.*, vol. 1, no. 3, pp. 415–428, Jul. 2002.

[19] D. P. Palomar, J. M. Cioffi, and M. A. Lagunas, "Uniform power allocation in MIMO channels: A game-theoretic approach," *IEEE Trans. Inf. Theory*, vol. 49, no. 7, pp. 1707–1727, Jul. 2003.

[20] T. M. Marzetta and B. M. Hochwald, "Capacity of a mobile multiple-antenna communication link in Rayleigh flat fading," *IEEE Trans. Inf. Theory*, vol. 45, no. 1, pp. 139–157, Jan. 1999.

[21] M. Biagi, "Cross-layer optimization of multi-antenna 4G WLANs," Ph.D. dissertation, Univ. Rome, Rome, Italy, 2005. [Online]. Available: http://infocom.uniroma1.it/~biagi/

[22] E. Baccarelli, M. Biagi, and C. Pelizzoni, "On the information throughput and optimized power allocation for MIMO wireless systems with imperfect channel estimation," *IEEE Trans. Signal Process.*, vol. 53, no. 7, pp. 2335–2347, Jul. 2005.

[23] Italian National Project. "*Wireless 8O2.16 Multi-Antenna mEsh Networks (WOMEN)*." [Online]. Available: www.womenproject.altervista.org

Enzo Baccarelli received the Laurea degree (*summa cum laude*) in electronic engineering, the Ph.D. degree in communication theory and systems, and the Postdoctorate degree in information theory and applications from the University of Rome "La Sapienza," Rome, Italy, in 1989, 1992, and 1995, respectively.

He is currently with the University of Rome "La Sapienza," where he was a Research Scientist from 1996 to 1998 and an Associate Professor in signal processing and radio communications from 1998 to 2003, and has been a full Professor in data communication and coding since 2003. He is also currently the Dean of the Telecommunication Board and a member of the Educational Board, both within the Faculty of Engineering. From 1990 to 1995, he was a Project Manager with SELTI ELETTRONICA Corporation, where he worked on the design of modems for high-speed data transmissions. From 1996 to 1998, he attended the international project AC-104: Mobile Communication Services for High-Speed Trains (MONSTRAIN), where he worked on equalization and coding for fast time-varying radio-mobile links. He is currently the Coordinator of the national project Wireless 802.16 Multi-antenna mEsh Networks (WOMEN). He is the author of more than 100 international IEEE publications and a coauthor of two international patents on adaptive equalization and turbo-decoding for high-speed wireless and wired data-transmission systems licensed by international corporations.

Dr. Baccarelli is an Associate Editor of the IEEE COMMUNICATION LETTERS, and his biography is listed in *Who's Who* and *Contemporary Who's Who*.

Mauro Biagi (S'99–M'05) was born in Rome, Italy, in 1974. He received the Laurea degree in telecommunication engineering and the Ph.D. degree in information and communication theory from the University of Rome "La Sapienza," in 2001 and 2005, respectively.

He is currently with the University of Rome "La Sapienza" and is involved with project managing activities for the Italian National Project Wireless 802.16 Multi-antenna mEsh Networks (WOMEN). His research interests include wireless communications (multiple-antenna systems and ultrawideband (UWB) transmission technology), dealing mainly with space-time coding techniques and power-allocation/interference suppression in multiple-input-multiple-output (MIMO) *ad hoc* networks, with special attention to game theory applications; transceiver design and UWB-MIMO applications; and wireline communications, particularly bit-loading algorithms and channel equalization for xDSL systems.

Cristian Pelizzoni was born in Rome, Italy, in 1977. He received the degree in telecommunication engineering from the University of Rome "La Sapienza," in 2003. He is currently working toward the Ph.D. degree at the University of Rome "La Sapienza."

His research interests include wireless communications, particularly space-time coding and game theory for *ad hoc* networks and multiantenna ultra-wideband systems.